INSTITUTE OF PHYSICS PUBLISHING JOURNAL OF PHYSICS D: APPLIED PHYSICS

J. Phys. D: Appl. Phys. **34** (2001) R23–R53 www.iop.org/Journals/jd PII: S0022-3727(01)07217-5

TOPICAL REVIEW

Micro-thermal analysis: techniques and applications

H M Pollock and A Hammiche

Department of Physics, Lancaster University, Lancaster LA1 4YB, UK

E-mail: h.pollock@lancaster.ac.uk

Received 21 December 2000

Abstract

The terms *micro-thermal analysis* and *micro-spectroscopic analysis* are used to include any form of localized characterization or analysis combined with microscopy that uses a near-field thermal probe to exploit the benefits of using thermal excitation. Individual regions of a solid sample are selected by means of surface or sub-surface imaging (atomic force microscopy and/or scanning thermal microscopy), so as to add spatial discrimination to four well-established methods of chemical fingerprinting, namely thermomechanometry, calorimetry, spectroscopy and analytical pyrolysis. We begin by describing the state of the art of scanning microscopy that uses resistive thermal probes, followed by an account of the various techniques of micro-thermal analysis.

Modern materials technology is increasingly concerned with the control of materials at the mesoscale. The ability to add an extra dimension of, say, chemical composition information to high-resolution microscopy, or microscopic information to spectroscopy, plays an increasingly useful part in applied research. Micro-thermal analysis is now being used commercially to visualize the spatial distribution of phases, components and contaminants in polymers, pharmaceuticals, foods, biological materials and electronic materials. This review outlines various applications that have been described in the literature to date, the topics ranging from multi-layer packaging materials and interphase regions in composites, to the use of the technique as a means of surface treatment.

Contents

0022-3727/01/090023+31$30.00

List of acronyms

AFM	atomic force microscopy
BLE	best linear estimate
CVD	chemical vapour deposited
DSC	differential scanning calorimetry
FFT	fast Fourier transform
(FT)-IR	(Fourier transform)-infrared
(GC)-MS	(gas chromatography)-mass spectrometry
L-CA	localized calorimetric analysis
(L)-DMA	(localized)-dynamic mechanical analysis
(L)-DTA	(localized)-differential thermal analysis
(L)-TA	(localized)-thermal analysis
(L)-TMA	(localized)-thermomechanical analysis
OPG	optical parametric generator
SThEM	scanning thermal expansion microscopy
SThM	scanning thermal microscopy
TASM	tomographic analysis for scanning microscopy
T_g	glass transition temperature

1. Introduction

In a wide variety of new forms of analytical instrumentation we see one common feature: quantitative analysis or physical characterization is combined with the ability to record microscope images, and thus to choose individual regions of an inhomogeneous sample for analysis. To give just one example, the rapidly expanding use of Raman microscopy arises from its ease of use, even with opaque or aqueous samples, as well as its ability to complement other analytical techniques such as Fourier transform infrared (FT-IR) spectroscopy.

The benefits of using *thermal excitation* have been exploited by several popular methods for the non-destructive characterization of solids at the macroscale. Any local disturbance of the structure, that results in a change in density, specific heat or thermal conductivity, may be detected by some type of thermal probe—often with higher sensitivity than by the use of optical, x-ray or electron-microscopical methods. Until recently, most materials technology has involved optimization of materials at the atomic scale (alloying) or at the macroscale (grain structure). In contrast, the development of nanocomposites is an example of how modern materials technology is also concerned with the control of materials at the mesoscale. Most microanalytical techniques lack the spatial resolution to operate in this regime. Consider the glass transition temperature (T_g) of an amorphous polymer, one of the most important parameters in polymer technology. At temperatures above T_g, the behaviour of a non-crystalline polymer material is either rubbery or viscous, depending on the molecular weight and by how much the temperature exceeds T_g. Below T_g, the polymer is glassy. The extent to which T_g may be affected by the confinement of the polymer matrix at a surface or interface is a topic of much current interest [1]. Likewise, the properties of blends and other inhomogeneous polymer materials may depend strongly on localized variations in crystallinity or T_g. The possibility of exploring such effects was one of the chief motives for the development of micro-thermal analysis.

Micro-thermal analysis, the subject of this article, was originally the name given to the combination of *localized thermal analysis* with near-field microscopy. In its wider sense as used here, it includes any form of localized characterization or analysis combined with microscopy, that uses a *near-field thermal* probe. Micro-thermal analysis was launched commercially in March 1998 (μTA™ Micro-Thermal Analyser (T A Instruments, New Castle, USA)), and two aspects of its development encourage the development of future variants.

(a) As in other forms of scanning probe microscopy, 'near-field' imaging[1] is achieved ('*scanning thermal microscopy*' (SThM)). We shall see that thermal imaging contrast is used to reveal spatial variations in the thermal conductivity and diffusivity of the sample, and that a particular advantage of SThM is its ability to detect *sub-surface* structure.

(b) Localized thermal/spectroscopic analysis builds upon this near-field thermal imaging technique, in order to add spatial discrimination to four well-established methods of chemical fingerprinting, namely *thermomechanometry*, *calorimetry*, *spectroscopy* and *analytical pyrolysis*. The same probe may be used in each version of the technique so that, as we shall describe, in principle it is possible to combine, in one instrument, a number of different modes of analysis—as well as surface topographic imaging by atomic force microscopy (AFM). The source of thermal excitation may be the near-field thermal probe itself, used both as a heater and as a thermometer ('active' thermal probe), for localized application of temperature programmes. For micro-thermal analysis, the *resistive probe* has proved to be the most useful device, and our technical descriptions concentrate on this type of detector. We then give examples of SThM that use resistive probes, followed by brief descriptions of the various techniques of micro-thermal analysis. Much of the published work has involved more than one such technique in combination and, for this reason, examples of the applications of micro-thermal analysis are described separately, in section 4 of this review.

2. Scanning thermal microscopy

A scanning thermal microscope, as generally employed, incorporates some or all of the following features:

- the probe as a near-field temperature detector;
- a source of heat—this may be external (e.g. incident electromagnetic radiation), internal to the sample (a buried hot region inside a chip) or, as mentioned above, may consist of the probe itself;
- a force transducer in the form of a cantilever, whose deflection senses the force that acts between the (thermal) probe and the sample;
- one or more feedback systems, in particular, force feedback and thermal feedback—accordingly, a scanning thermal microscope generally acts also as an atomic force microscope;
- the remaining components that are needed in the construction and operation of an atomic force microscope. The functions involved include actuators for spatial

[1] As opposed to traditional variants of microscopy in which the spatial resolution depends on wavelength, as determined by the relevant *far-field* optics.

scanning, a system to measure cantilever deflection, display and analysis software, etc.

As with a standard atomic force microscope, the height of the probe above the surface being scanned is generally controlled by a feedback system that maintains constant the force between probe and surface; the probe height is used to create topographic image contrast, quite independently of the process of temperature measurement. At the same time, the temperature signal from the same probe is used to generate a thermal image. This contains information that will depend upon a number of factors, including the nature of the heat source employed.

A variety of types of thermal probe have been developed. The first SThM modes were developed by Wickramasinghe and colleagues, using *thermoelectric* signals. The probe was a specially made coaxial tip that formed a fine thermocouple junction. Either the sample was heated by means of a laser, or the probe or the sample were heated electrically. The original set-up [2] was developed as a surface profiler (or an alternative to the subsequently-developed atomic force microscope). The signal allowed the heat flow between probe and sample across the air gap to be monitored and used as a means of maintaining the gap width during scanning, regardless of any variations in the thermal properties of the sample. The same device was then used to map spatial variations in temperature [3], over an inhomogeneous internally heated sample. They achieved a spatial resolution of the order of tens of nanometres, and a thermal resolution of about a millidegree. Nonnenmacher and Wickramasinghe [4] also achieved sub-surface thermal imaging of electrically conducting samples, with the thermocouple junction being formed by the tip/sample contact itself, and the cantilever being heated by a laser beam. Majumdar *et al* [5] used a more simple design of thermocouple tip, and standard force feedback to maintain tip/sample contact as in other forms of AFM, so that the topographic profiling was decoupled from the process of temperature measurement.

In one type of SThM, a tip/sample tunnel junction, acting as a thermocouple, was formed by bringing an electrically conducting probe and sample within tunnelling distance [6]. Alternatively one may measure the contact potential between conducting probe and sample, and make use of the strong temperature dependence of this contact potential between two metals under ambient conditions [4], in order to obtain scanning probe images showing thermal contrast. Thin-film temperature sensors have been grown onto commercially available cantilever AFM probes [7]. An important step forward exploited the temperature-induced deflection of a bimaterial cantilever; if an AFM cantilever is coated with a film of a second material, mismatch in the thermal expansion coefficient between the results of the two materials produces the cantilever deflection that is then sensed [8, 9]. In one development, reflectance thermometry [10] exploits the fact that the optical properties of many materials are temperature-dependent. This means that scanning near-field optical microscopy may be used to detect the changes in collected radiation power caused by any pre-existing temperature variations over the surface of a biased interconnect, for example. The list ends with electrical resistance thermometry, described in the following section, where we outline the way in which sub-surface detail detected in SThM corresponds to variations in heat capacity or thermal conductivity.[2]

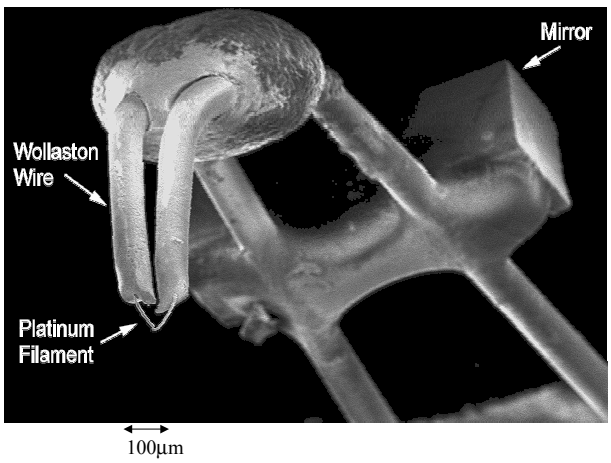

Figure 1. Wollaston probe, as developed by Dinwiddie *et al* [11] and subsequently used by Balk *et al* [14] and by Hammiche *et al* [13]. The temperature is sensed by the apex of a V-shaped 5 μm diameter platinum/10% rhodium wire. Typical values of spring constant range from 5–20 Nm^{-1}. These probes are remarkably robust, both mechanically and electrically, and have been heated to temperatures of around 1000 °C. (After [15], copyright 2000, with permission from Elsevier Science.)

2.1. Thermal microscopy using resistive probes

Resistive probes have one great advantage in applications requiring more than topographic and thermal imaging—they may be used in active mode, thereby acting as a self-contained device for the supply of heat as well as temperature measurement. Consequently, they may be used for localized thermal analysis (L-TA) as well as AFM/SThM, as we describe later. For this reason, the coverage of this review is restricted to work that uses resistive probes. The type of sensing element often used in near-field *resistance thermometry* consists of the apex of a fine V-shaped wire (figure 1), known as the *Wollaston probe* after the type of silver-sheathed noble metal wire from which they are made. Recently, a high-resolution micromachined version has been developed (figure 2). From the shape of the sensing element, this has been described as the *bow-tie probe*.

The resistive probe is capable of performing three functions: it exerts a force on the sample surface; it acts as a highly localized heat source, either constant, modulated or ramped; and it measures heat flow. Probes can be used in either of two operating modes [11, 13]:

- constant temperature mode, requiring temperature feedback, with self-heating;
- constant current mode—a small current is then passed through the probe which then acts as a thermometer.

In the constant temperature (active, self-heating) mode, the thermal element is used as a resistive heater and forms part of a Wheatstone's bridge circuit. When the probe contacts

[2] In a recent review [12], Majumdar describes the above modes of operation in detail and describes how SThM is used in studies of physical phenomena at small lengths and timescales, ranging from thermal transport in optoelectronic devices to temperature distributions in vertical cavity surface emitting lasers.

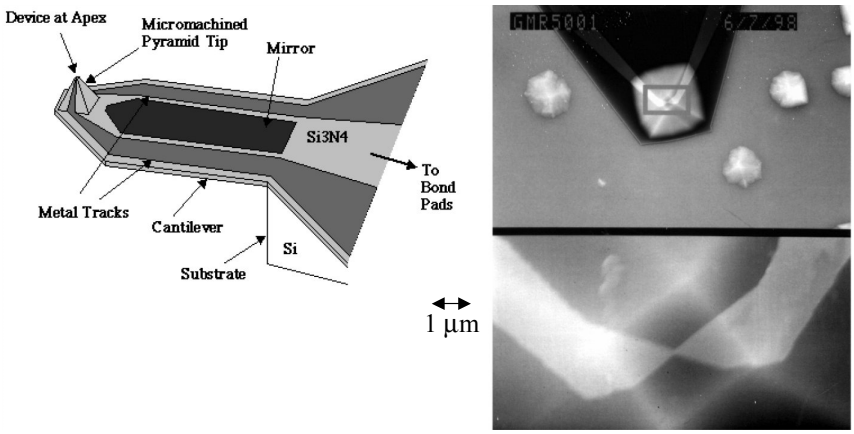

Figure 2. Micromachined 'bow-tie' probe [16–18]. The entire probe, including cantilever, silicon nitride pyramidal tip and palladium resistor, is produced in batches of 240 and 60 (full or $\frac{1}{4}$ wafer) using photolithography, potassium hydroxide etching and multiple-level electron beam lithography. Here, the resistive element is formed by patterning an abrupt taper in a palladium wire that runs across the flattened apex (2.5×2.5 μm square) of the 20 μm high pyramid. Typically it measures 100 nm at its narrowest point, but the taper can be varied in size and a minimum width of 35 nm has been demonstrated. Electrical lead-ins to the resistive element are patterned along the cantilever and up the sides of the pyramid. (After [17], copyright 1999 American Vacuum Society.)

successive regions of the sample surface that may differ in their thermal properties, varying amounts of heat will flow from the probe to the sample. However, the probe heating circuit uses a feedback loop to adjust the current through the probe as necessary to keep the probe resistance, and hence the temperature, constant. The required feedback voltage is used to create contrast in the thermal image. The power involved may be calculated from the bridge output voltage and is affected by several factors including the probe/sample contact area, the temperature difference between probe and sample, and variations in the local thermal conductivity of the near-surface regions of the sample.

2.1.1. Resolution and contrast. We thus see that the images obtained by use of thermal probes show either topographic or thermal contrast, and in the latter case both sub-surface as well as surface detail. In many instances, topographic resolution will be just as important as thermal resolution; for example, in a case where the probe is to be used just to perform L-TA on a region that is defined clearly enough in the topographic image. However, given the non-ideal geometry of the thermal probe, in topographic images the resolution is never as good as is obtained using standard AFM probes. The remaining question is that of the quality of the thermal image, in particular the following.

(a) Detection of fine detail—what is the smallest feature on the sample surface that is revealed?
(b) Spatial resolution—what is the smallest separation at which the gap between two similar surface features is revealed?
(c) Contrast in unprocessed thermal images is a convolution of topographic detail with true spatial variations in thermal properties (hence the 'deconvolution problem', to be discussed below). For fine near-surface detail in a given case, does the contrast in the thermal image correctly correspond to these variations? The finest detail for which this is true could be called '*thermo-spatial resolution*'.
(d) Sub-surface detail—how rapidly does the performance as detailed in (c) degrade as we increase the the depth of the detail to be detected or resolved?

In each case, the answer will of course depend upon how far apart are the values of thermal conductivity of the neighbouring regions that are to be resolved. In addition, the resolution depends upon the mechanism of heat transfer between probe and sample. In principle such mechanisms will include direct solid–solid conduction, conduction and convection through the ambient gas, heat transfer through any adsorbed film of moisture, and radiation. The first substantive study of thermal transport on the scale of a few micrometres was described by Dransfeld and co-workers [19, 20]. Their primary concern was the contribution of radiative heat transfer through proximity effects, such as thermally-excited non-propagating surface modes of charge fluctuation. In fact, they concluded that such effects should make an insignificant contribution to thermal coupling in SThM at room temperature, although it could become significant in ultra-high vacuum.

Until recently there has been little or no firm evidence [12] for *direct solid/solid conduction* as a dominant heat transfer mechanism. However, most of the relevant studies involved thermocouple probes whose heat capacity is much smaller than that of the Wollaston resistive probe, in which case the effect of the thermal shunt produced by heat flow through the air surrounding the tip is relatively more significant. Some recent experiments, by Gomès *et al* [21] and by Gorbunov [22] using resistive probes, have shown that for samples with high thermal conductivity (some metals) there is an abrupt increase in heat flow on contact, even at probe temperatures previously shown to be high enough for any water meniscus to have evaporated.

Two other contributions to the heat flow can be important, involving transfer through a liquid phase or through the surrounding air (or gas). The work of Luo *et al* [23–25] has shown that *liquid–film conduction* can be the dominant tip–sample heat transfer mechanism, for thin-film probes at least. The probe temperature will affect the thickness of the liquid film bridge that forms between probe and sample

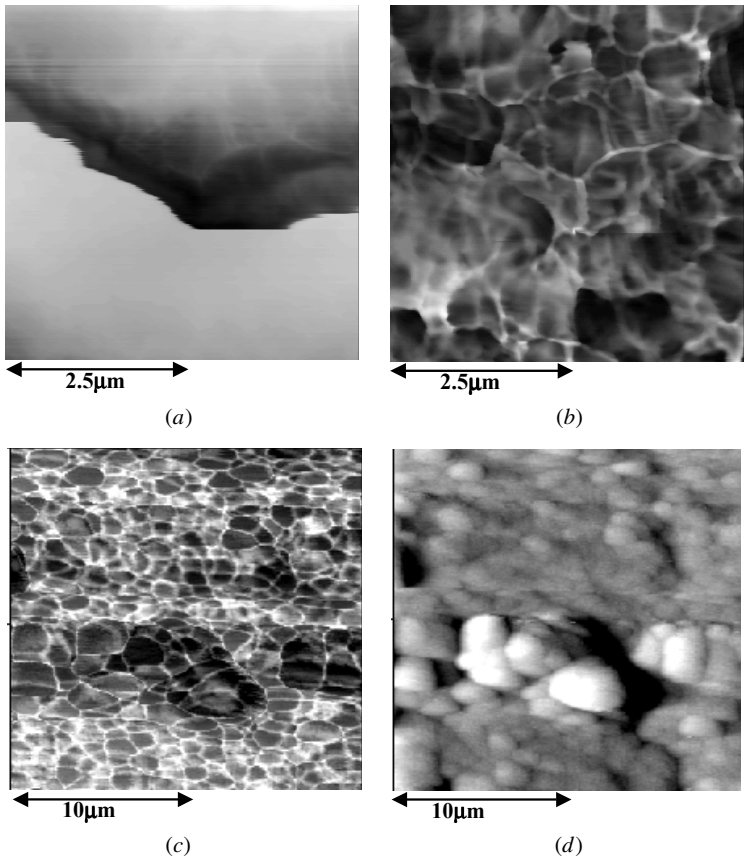

Figure 3. Examples of thermal images showing contrast that is independent of sample roughness: (*a*) topographic image of polished sintered ceramic surface ($MgSiN_2$)—a groove of about 300 nm in depth is clearly visible; (*b*) as (*a*), but thermal image, with a probe temperature of 150 °C—clearly distinguishable crystals are seen, and the thermal contrast is entirely unaffected by the deep groove; (*c*) thermal image of thin coating of gas phase-deposited SnO_2 on Al, with a probe temperature of 250 °C. Similar features to (*b*) are visible in (*c*) and (*d*)—scanning speed of 60 μm s^{-1}, probe temperature of 250 °C. As with $MgSiN_2$, the grain size and grain boundaries are clearly observable. (*d*) As (*c*), but a topographic image—resolution is poor compared with that of the thermal image. (After [27], and [28], copyright 2001 H T Hintzen, and R Groenen.)

when the contact is made in air at non-zero relative humidity. Majumdar [12] has analysed how the probe radius affects the relative values of the liquid and gaseous contributions, and the factors that determine the optimum value of tip radius under a given set of operating conditions.

An important point is the question of *topography-related artefacts*. With most types of sample, 'thermal contrast' is indeed affected by topography. False heat flow peaks (increased tip/sample contact area) and troughs (reduced contact area) tend to be produced by valleys and hills, respectively, on the sample surface. In addition, as shown by Fischer [26], even when the contact force is carefully controlled, there can be significant wear of the probe, leading to unwanted variations in contact area. Other factors can contribute to false thermal contrast, if for example the liquid bridge conduction mechanism outlined above applies. Nevertheless, there are good examples of images of non-flat surfaces in which unambiguous thermal contrast appears that is independent of topography (figure 3). We return to this point later.

2.1.2. Modelling. Despite the above complications, progress has nevertheless been made in developing models that are sufficiently general to be helpful in indicating (a) theoretical limits to resolution and depth-sensitivity, and (b) possible approaches to improved probe design.

It is simplest to consider first the dc case when no temperature modulation is used. The model of Hammiche *et al* [13] considered the probe–air–sample system as a series of fine strips, and they allowed a finite amount of heat to escape from the sides of each strip. The system consisted of the source (regarded as planar), the air gap between source and sample, the sample material, a buried inclusion of a different material, and the underlying semi-infinite support. The resulting heat equation for the dc case was solved in one dimension with appropriate boundary conditions. The model was then used to simulate heat flow from probe to sample with inclusions buried at different depths, and the results were compared with experiment. The case of two inclusions with a given lateral separation was also considered. It was concluded that depth detection, and differentiation of thermal inhomogeneities, depend on the temperature resolution of the instrumentation and the minimum detected heat flow. This, in turn, is affected by the probe shape and for the Wollaston probe is of the order of 1.5 μm at the surface: with sharper tips it should increase by an order of magnitude. At depths of a few ($\leqslant$10) μm, the resolution degrades by a factor of half an order of magnitude.

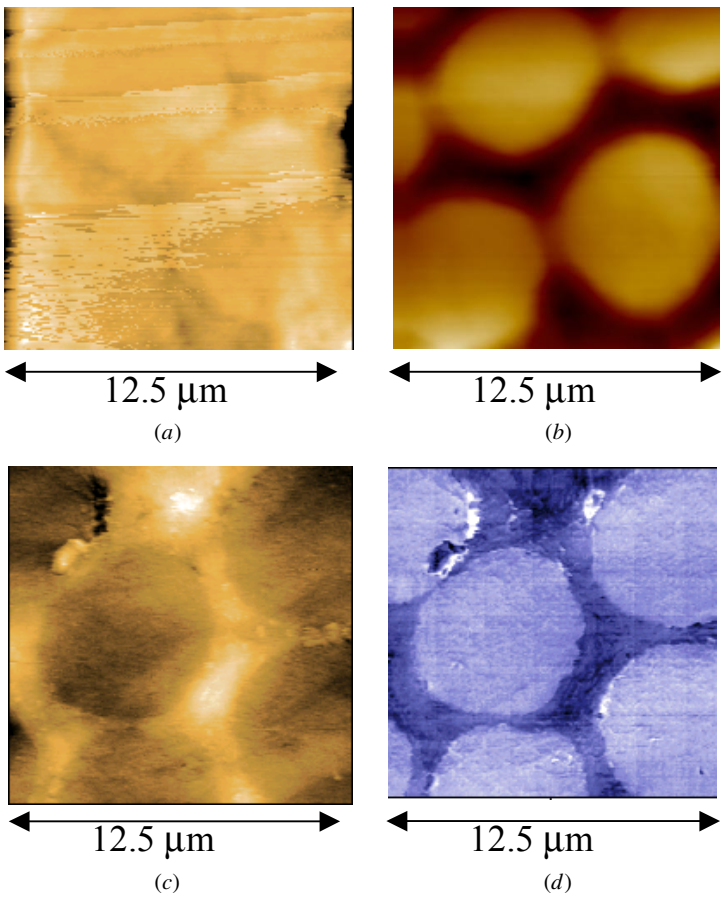

Figure 4. Polished cross section of carbon fibre–carbon composite, with the carbon fibres embedded in bitumen, which is then converted to a carbon matrix by heat treatment. (The sample was prepared by Dr C Blanco and Dr S Appleyard, Department of Materials, Leeds University; imaging by Dr M Conroy, Lancaster University.) The topographic images (left) confirm that the surface is flat to within 200 nm; the fibres, having higher thermal conductivity, are revealed in the dc thermal images (right). Images obtained using bow-tie probes (bottom row) show finer detail than is resolved by Wollaston wire probes (top row). (After [32], copyright 2001 John Wiley and Sons.)

2.1.3. Contrast and spatial resolution in practice. It is perhaps surprising that with the Wollaston probe in the form of a bent 5 μm diameter wire, sub-micrometre spatial resolution is achieved. Nevertheless, Balk *et al* [14] have published ac thermal images of contact areas of a GaAs-based tunnelling diode, indicating that this type of probe can distinguish detail as fine as 30 nm in practice. From figure 4, we see that for very flat samples it is possible to obtain true thermo-spatial resolution of the order of 100 nm. Our early publications [13,30,31] described work on polymer blends in which two or more components were distinguished in the thermal image. As expected, the 'bow-tie' type of micromachined probe mentioned above gives much improved spatial resolution. Examples of the comparative performance of the two types of resistive probe are shown in figures 4 and 5. The chief conclusions from such comparisons are as follows.

(1) Anisotropic effects. When Wollaston images are being recorded, during each line of the scan the probe moves in the direction (x) lying within the plane of the loop of wire. The resolution is noticeably higher in the perpendicular direction (y). For the bow-tie probes in particular, there can be a large difference in *topographic* contrast between forward and reverse scans, if the probe is aligned relative to the sample surface in such a way that the region of the probe surface involved in mechanical contact varies with scan direction. This does not apply to the thermally active element.

(2) Spatial resolution and image sharpness. It is possible for the thermal image to reveal much finer detail than the topographic image. In figure 3(b), not only are individual grains of sintered $MgSiN_2$ crystals clearly distinguishable in the thermal image, but the grain boundaries also appear as a sharp change in contrast. Figures 3(c) and 3(d) show a thin inorganic coating (SnO_2) on aluminium; the resolution in the topographic image is poor, but in the thermal image the grain size and the grain boundaries are clearly observable.

The bow-tie probes show even finer detail, for example in images of model samples made from 100 nm thick layers of poly(methyl)methacrylate (PMMA) on silicon. With a flat carbon–carbon composite sample (figure 4), the bow-tie images show fine detail within the matrix, while no comparable detail is resolved in the Wollaston image.

(3) True thermal contrast between materials. We have seen (figure 3) that contrast in the thermal images can be independent of topography. In order to explore the conditions necessary for this to be so, Mills *et al* [33] have used both

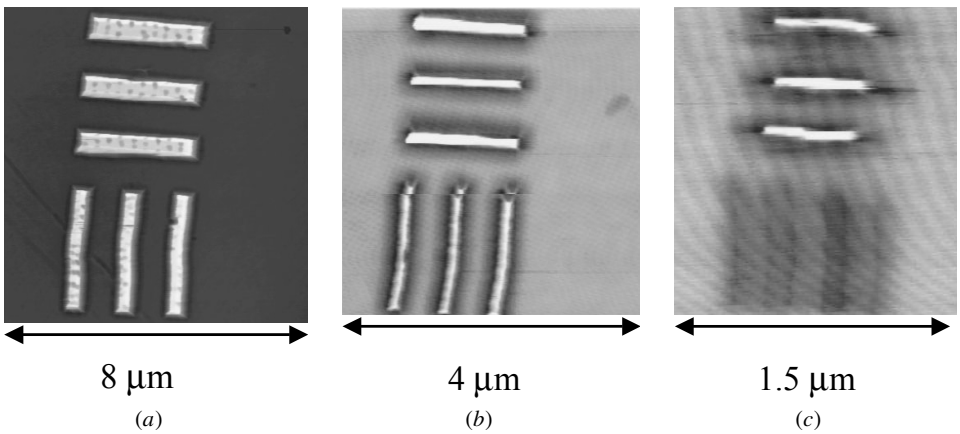

Figure 5. Bow-tie probe dc thermal images of a model sample consisting of silica coated with a discontinuous layer of PMMA of a thickness of 500 nm. (The sample was prepared using photolithography by Dr G Mills, Glasgow University; imaging by Dr A Hammiche, Lancaster University.) Gaps in the PMMA appear as lines, exposing the silica which has higher thermal conductivity. In the three areas shown, the linewidths and spacings have been successively reduced in the order *a–b–c*. The appearance of the silica changes from white (genuine) to dark (misleading), as the linewidth decreases. Lines of widths down to 200 nm are still detected, and true thermal contrast is seen for this linewidth, but only when the scan direction (left to right) is parallel to the lines. For the perpendicular scan direction, the silica contrast starts to deteriorate at a 500 nm linewidth. At a 100 nm linewidth, correct thermal contrast has disappeared. As with the Wollaston probe (figure 3(*b*)), thermal images tend to give sharper topographic detail.

types of probe to image a range of model samples consisting of discontinuous thin PMMA layers in the form of islands (strips or discs) of different spacings, deposited onto silica substrates. The correct thermal contrast (higher thermal flux for contact with silica than with PMMA) is seen, provided that the probe is sharp enough to reach between the islands and make contact with the silicon (figure 5). Otherwise, the thermal signal from the 'valley' regions between the islands will give a misleading indication of the local variation in thermal conductivity.

In the next section we give examples of the additional information obtained by means of temperature modulation, together with the relevant theoretical models.

2.2. Use of temperature modulation

In SThM the chief motive for using temperature modulation is to control the depth, below the sample surface, from which the information is derived. The same principle has long been used in a wide range of photothermal techniques, where the modulation may take the form of chopped laser illumination, for example. When an active thermal probe is used, modulation can be superimposed directly on the heating current itself. The depth-sensitivity depends on the fundamental *evanescent* property of thermal waves; if a plane wave is incident normally upon a sample in the form of a half-space, the equation describing the attenuation of temperature with distance z contains the factor $\exp(-z/L_1)$, where the thermal diffusion length L_1 is proportional to the square root of the diffusivity μ of the material divided by the modulation frequency [34]. In a typical polymer, for example, the value of μ is 1×10^{-7}, so that at a modulation frequency of 10 kHz, the value of L_1 is 4.5 μm. Because of the small size of the probe and of the region of the sample being heated at any one time, heating and cooling may be very rapid. Gmelin *et al* [35] have tabulated typical values of temporal resolution achieved by the use of the various types of thermal probe. The time constants that characterize the latest micromachined probes have not yet been accurately measured, but are estimated to be in the region of a few tens of nanoseconds. Even with the Wollaston probe, the rate of data acquisition is high, and temperature modulation frequencies in the hundreds of kilohertz range may be used. Typical values of modulation amplitude in practice range from 1–10 °C (figure 6).

2.2.1. Ac imaging. A second feature of the images obtained using temperature modulation ('ac imaging') is that the subsurface detail detected corresponds to variations in heat capacity as well as in thermal conductivity (k_c), and this raises the possibility of quantitative determination of values of both these parameters for individual regions of an inhomogeneous sample (we return to this topic in section 2.4). Several groups have employed ac imaging to explore thermal diffusivity variations in materials [14, 37, 38].

As shown in figure 6, four images of a sample may be obtained simultaneously: topographic, dc thermal, ac thermal (amplitude) and ac thermal (phase). There has recently been considerable interest in attempting to model the imaging processes in detail. A successful model would be able to predict the sensitivity of a particular design of thermal probe for detecting spatial variations in k_c and μ, and ideally to allow their absolute values to be derived. The relevant models allow for the fact that the simple one-dimensional attenuation parameter above (L_1) cannot provide a valid basis for describing the temperature distribution in a three-dimensional (3D) sample in contact with a probe of sub-micrometre dimensions. In practice, clearly the penetration depth of the thermal wave into a 3D sample will be less than L_1; the temperature will fall away rapidly as we move away from the heat source. This will be true even when no modulation is used, in which case we may characterize this decay in temperature amplitude as an effective zero- frequency diffusion length L_0. Using a finite-element method (FEM), Smallwood *et al* [39] have found that this length is almost independent of material properties and is a function of the probe–sample contact area (A) alone.

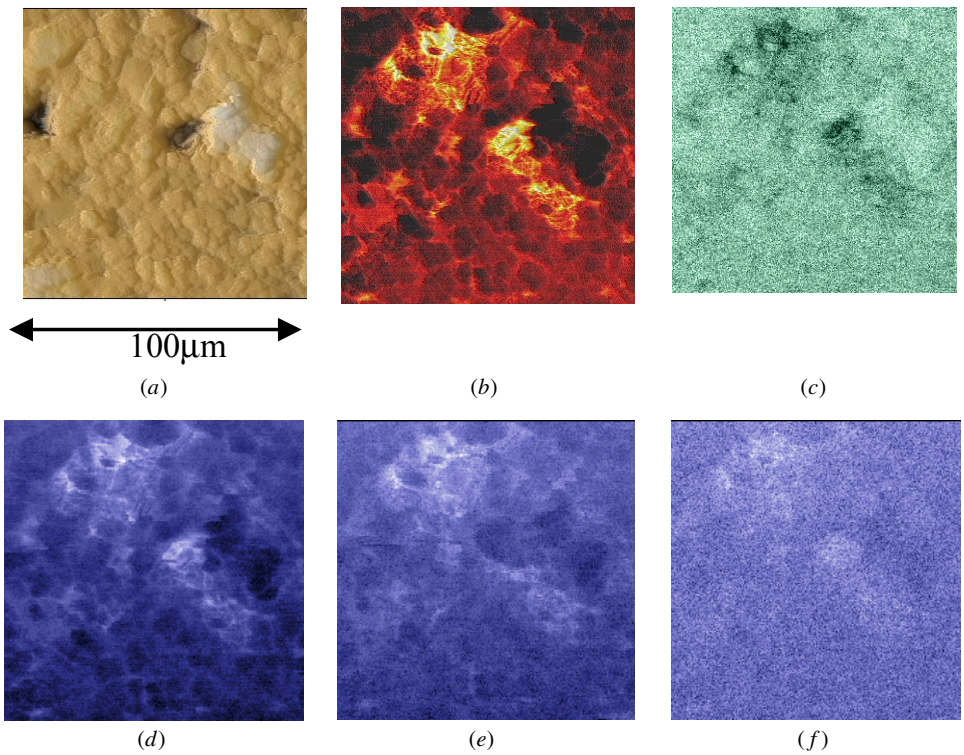

Figure 6. Images of the surface of a paracetamol tablet: (*a*) topographic, (*b*) dc thermal, and (*c*) ac phase thermal image at 10 kHz; ac amplitude thermal images, at modulation frequencies of (*d*) 10 kHz, (*e*) 30 kHz, and (*f*) 100 kHz. (After [36], copyright 1999, with permission from Elsevier Science.)

It is necessary to characterize the situation that involves both temperature modulation and 3D heat flow. For this purpose we define an effective diffusion length L_ω, and it proves possible to express this in terms of L_1 and L_0. The 3D FEM analysis leads to the following simple approximation:

$$L_\omega^2\left(\left[L_0^{-4}+4L_1^{-4}\right]^{1/2}+L_0^{-2}\right)=2. \tag{1}$$

It follows that at low frequency ($L_1 > L_0$), there is no significant effect of frequency upon L_ω, which tends towards L_0. At very high frequency ($L_1 \ll L_0$), L_ω will tend towards L_1 if either the modulation frequency, or the probe size (and L_0), is very large. There will therefore be a trade-off; if we want frequency discrimination it may be necessary to use a probe of a large diameter, which will give an increased scan depth but will degrade the spatial resolution. In principle, it would be possible to synthesize a virtual large probe from a number of measurements made by a smaller probe. In the following section, we discuss how this result plays an important part in the development of true tomographic reconstruction.

A very simple spherical symmetry model gives a semi-quantitative illustration of how local variations in both thermal conductivity and diffusivity must contribute to the signal that determines contrast in ac thermal images. We take the probe to be a spherical heat source, of radius r_0, emitting thermal waves isotropically into the surrounding sample which fills the remaining space. It is then possible to derive an analytical formula for the heat flow as well as the temperature distribution. Firstly, it is necessary to solve the differential equation [40] for the spatial (radial) component of temperature, $R(r)$:

$$\frac{\mathrm{d}^2R(r)}{\mathrm{d}r^2}+\frac{2}{r}\frac{\mathrm{d}R(r)}{\mathrm{d}r}-\frac{\mathrm{j}\omega_n}{\mu}R(r)=0 \tag{2}$$

where r is distance from the origin (the centre of the probe), μ is diffusivity,[3] and ω_n is the frequency of the thermal wave (taking values 2ω, 0 and -2ω if the probe is resistively heated by means of a current of frequency ω). With the boundary condition that at the probe/sample interface ($r = r_0$) the temperature–amplitude has some fixed value (Θ_0), the solution to this equation gives the value of temperature $R(r)$ at any point. The heat flow rate is:

$$\sum_{n=1,2,3}\left(4\pi k_\mathrm{c}r_0^2\Theta_0\frac{\mathrm{d}R(r)}{\mathrm{d}r}\hat{T}_n\left(\omega_n\right)\exp\left(\mathrm{j}\omega_n t\right)\right) \tag{3}$$

where for $n = 1, 2, 3$ we have $\omega_n = 2\omega, 0, -2\omega$ and $\hat{T}_n = \frac{1}{2}$, 1, $\frac{1}{2}$. When we omit the dc term this flow rate becomes:

$$\begin{aligned}2\pi k_\mathrm{c}r_0\Theta_0\Bigg(&\sqrt{2}\cos\left[2\omega t-r_0\sqrt{\frac{\omega}{\mu}}-\frac{\pi}{4}\right]-2r_0\sqrt{\frac{\omega}{\mu}}\\&\times\cos\left[2\omega t-r\sqrt{\frac{\omega}{\mu}}\right]-\exp\left[2r_0\sqrt{\frac{\omega}{\mu}}\right]\\&\times\Bigg(\sqrt{2}\cos\left[2\omega t+r_0\sqrt{\frac{\omega}{\mu}}-\frac{\pi}{4}\right]\\&+2r_0\sqrt{\frac{\omega}{\mu}}\cos\left[2\omega t+r_0\sqrt{\frac{\omega}{\mu}}\right]\Bigg)\Bigg).\end{aligned} \tag{4}$$

We see that at frequencies low compared with μ/r^2, the exponential term just becomes 1 and, as expected, the

[3] Defined as $k_\mathrm{c}/(\rho C_\mathrm{p})$, where k_c, ρ and C_p are thermal conductivity, density and specific heat, respectively.

modulated heat flow varies more strongly with k_c than with μ (the dc component varies simply as $k\Theta_0 r_0$). At frequencies high compared with μ/r^2, the exponential term dominates and the modulated heat flow amplitude varies as:

$$2\pi k_c \Theta_0 r_0^2 \sqrt{\frac{\omega}{\mu}} \exp\left[2r_0\sqrt{\frac{\omega}{\mu}}\right]$$

so that variations in frequency and diffusivity have a much greater effect than at low frequencies. While it remains true that at lower modulation frequencies the technique is 'looking' deeper into the sample, it is important to appreciate that variations in conductivity as well as diffusivity must contribute to the image contrast.

Thermal fin theory [12] has been used to estimate the heat loss through the leads to the probe and to show that when, for example, a polymer is being imaged at a modulation frequency of 10 kHz, the ac conductance to the leads exceeds the ac conductance to the sample by several orders of magnitude. In recent work at Reims University [41–43], a rigorous model has been developed to describe ac thermal coupling between probe and sample in SThM, taking into account the temperature variation along the length of the probe. The probe is taken as a simple cylindrical thermal fin, incorporating a planar distributed source of thermal waves in one dimension. This is then linked to a two-layer medium (the air gap, and the 3D sample as a staircase multilayer). The resulting equations were solved by a method of plane wave spectra in each of the homogeneous layers describing the system, and gave the entire ac temperature field within the sample. A recursive numerical evaluation using two-dimensional (2D) fast Fourier transform (FFT) was used to generate data on a series of hypothetical samples, giving the value of thermal coupling (i.e. the ratio of probe temperatures with and without the sample being present), as a function of sample diffusivity. Curves of temperature amplitude ratio against probe–sample separation are S-shaped, and tend to a common value at larger separations where the air gap is larger than the thermal diffusion length. When water instead of air is the coupling medium, the coupling increases. One limitation of the model is that, within its constraints, the thermal fin hypothesis is valid only for thermal diffusion lengths that exceed the probe radius and the thickness of sample material of interest; in practice, this implies modulation frequencies below some tens of kHz. A further point is that the FFT procedure implies fine discretization for the 3D sample, with a correspondingly large computer memory requirement for high frequencies.

The theory was also used to model the ac imaging of samples containing buried inhomogeneities of finite size, modelled as small thermal resistances embedded in the sample [42, 44]. In this case, the required FFT algorithms involved successive approximations. The amplitude and phase of the temperature signal were calculated for suitable values of thermal resistance, depth and spacing, and the model confirms that the inhomogeneities are detected up to a depth which is of the order of a few tens of micrometres.

2.2.2. Thermal impedance tomography. In the general area of process control, many manufacturers have particular interest in inhomogeneous composites. They may wish to measure parameters such as the size and dispersion of embedded particles, and the thickness and uniformity of thin surface layers. Often they have access only to the surface of the material, and need to infer depth information from surface measurements. In the previous section we have seen how the use of temperature modulation can provide semi-quantitative detection of features, such as particles buried below the sample surface, and which distort the temperature field. Important questions remain unanswered. If an inclusion is detected, how large is it? How deeply is it buried? Are there multiple inclusions? Recently, a possible route to fully quantitative *tomographic* characterization has been described, known as thermal impedance tomography or TASM (tomographic analysis for scanning microscopy).

The problem is to reconstruct some property of the interior of a material when measurements are confined to the surface. In recent work [39], 3D medical imaging techniques (originally developed for electrical impedance tomography in human subjects [45]) have been adapted to SThM, as a step towards the generation of 3D thermal images of polymeric materials from measurements made on a planar surface of the material. For TASM, the general approach is first to encode 3D information in a 2D space (the 'forward problem'), and then to find an algorithm for solving the inverse problem of determining the 3D information from the encoded 2D data.[4] To solve the inverse problem it is necessary to find the inverse of a very large 'sensitivity matrix'. The generation of a 3D image of thermal conductivity and diffusivity requires five independent parameters to be measured. These are the rectangular coordinates of the probe position on the surface, the modulation frequency of the power input to the probe (which determines the penetration depth of the evanescent thermal wave), and the amplitude and phase of the resulting temperature signal.

Thus the method is as follows:

- Two-dimensional information is collected over a range of modulation frequencies.
- A sensitivity matrix is constructed by calculating the change in the measured property, for every measurement site, of an incremental perturbation in the flow of heat through each voxel. This matrix ($\mathbf{S}$) is generated by modelling the forward problem (solving the Helmholtz equation) for a *uniform isotropic* medium, expressed as a set of linear equations:

$$\boldsymbol{t} = \mathbf{S}\boldsymbol{k} \tag{5}$$

  where the vector $\boldsymbol{k}$ represents the incremental change in 3D thermal properties (in each of the discrete elements) required to perturb the heat flow, and $\boldsymbol{t}$ is the corresponding change in measured 2D surface temperature as a function of frequency. We note that once the correct matrix has been found, for such a medium the resulting temperature distribution should of course be uniform in space.
- This sensitivity matrix is then inverted.
- The 2D data is then multiplied by this inverse, which from the above equation gives the required distribution of thermal properties (3D image).

[4] We can make the analogy with x-ray tomography, where the simplest algorithm is that involved in back-projection—very simple given that the directions of propagation are straight lines. In the case of TASM, that is not so!

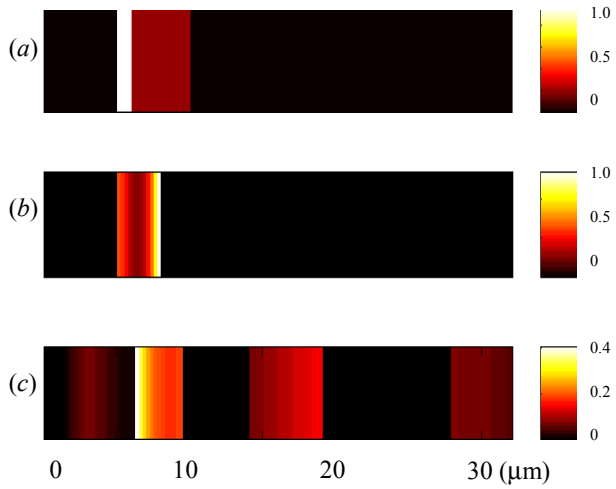

Figure 7. One-dimensional BLE reconstruction of the GCL film: 5 μm PET, 40 nm Al, 5 μm adhesive, 25 μm PET. The x-scale shows the depth below the surface, and the contrast scale gives values of the thermal properties vector $\boldsymbol{k}$, referenced to bulk PET: (*a*) schematic representation of the actual sample; (*b*) BLE reconstruction of simulated sample; (*c*) BLE reconstruction of real sample using experimental data. (After [39], copyright 2001, with permission from Elsevier Science.)

The forward problem was solved by implementing the finite-element analysis software mentioned above, but the sensitivity matrix is *ill-conditioned* (near-singular) and very large (e.g. for 150 × 150 × 40 volume elements and eight frequencies, there are 1.5×10^{12} elements, or 6000 GB). It was found that it would need 20 000 years of computing time to invert, with a few hundred hours to compute the image. Fortunately, in order to solve the inverse problem, it proved possible to develop an iterative image reconstruction algorithm—best linear estimate (BLE)—which does not require storage of the full sensitivity matrix nor its explicit inversion. This algorithm addresses the ill-conditioning by explicitly considering the inaccuracies in the vector of the measured temperature data, treating these inaccuracies as random noise. An iterative search technique is used to seek the 'best' (in a stochastic least-squares sense) linear reconstruction of the thermal properties vector $\boldsymbol{k}$. Intermediate solutions of $\boldsymbol{k}$ are generated, and iteration continues until variations in $\boldsymbol{k}$ between iterations are smaller than some decision value. The typical time for the solution is ten minutes.

This approach has successfully confirmed the relation between diffusion length and probe dimension described in the previous section, although it does not yet allow for complications such as thermal impedance between probe and substrate. The tool has been applied to a virtual material, with results that agree with analytical calculations. Work with real samples has so far been limited to layered structures, the data being collected using ac SThM over the modulation frequency range 10 Hz to 10 kHz. The real and simulated images have been reconstructed using the BLE method with 128 independent frequency measurements which results in a 128 element one-dimensional image. Figure 7 shows a typical result.

2.3. Scanning thermal expansion microscopy

Varesi and Majumdar [46] have described a method of thermal expansion imaging, termed *scanning Joule expansion microscopy*, in which Joule heating is applied by means of a modulated electric current passed through an electrically conducting sample. A conventional AFM probe is used to detect the resulting modulated thermal expansion for purposes of imaging. A related technique, *scanning thermal expansion microscopy* (SThEM) [47], employs a similar principle but does not require the sample to be electrically conducting; once again, the active resistive thermal probe is used to provide localized heating. The resultant localized temperature modulation is used to generate thermal expansion, which is detected and used to generate image contrast. The attraction of such an imaging method lies in the fact that for many materials, thermal transitions have a greater affect upon thermal expansion coefficient and elastic modulus than upon thermal conductivity or heat capacity. These localized versions of thermomechanical modulation have proven useful in the detection of thermal events.

In SThEM, as the probe is scanned across the surface of the specimen at a constant underlying force, an external source is used to apply an alternating current of chosen frequency ω_c to the probe. The ac current modulates the tip temperature at $\omega = 2\omega_c$. Heat transfer from the tip to the specimen results in thermal expansion of the surface at the same frequency. This causes modulated deflection of the probe height which is detected using the AFM z-axis feedback system. The amplitude and phase shift (with regard to the heating current) of the localized expansion are recorded, using a lock-in amplifier, by monitoring the modulated deflection of the probe, to create images. Three images are recorded simultaneously: topography, amplitude of surface expansion and phase of surface expansion.

Scanning thermal expansion microscopy has been shown to give useful contrast over a frequency range of 15–2000 Hz, in images of a resin/polyethylene terephthalate (PET) composite, when either the Wollaston probe or the micromachined probe were used. Amplitude images give more contrast than phase images, and the amplitude of the surface expansion is larger for the resin than for the PET, indicating a higher coefficient of thermal expansion. The depth of material contributing to the measured thermal expansion was estimated from values of the amplitude of the thermal expansion produced at the lowest modulation frequencies (15 Hz or below; 2.0 nm and 4.5 nm for the PET and the resin respectively), resulting from a Wollaston probe temperature amplitude of 10 °C. Using measured values of the thermal expansion coefficients of the two materials, a value of 2.5–3.1 μm was obtained for the effective depth of the material being heated locally during the SThEM experiment.

It is possible that the method could be developed to provide quantitative mapping of spatial variation in thermal expansivity. It would be necessary to deconvolute the role of thermal conductivity (using data from unmodulated thermal images) and diffusivity (which, together with modulation frequency, determines the depth of penetration of the thermal wave). The contribution of the probe would be calibrated using a reference material of known thermal properties.

2.4. Measurement of the absolute thermal properties of materials on a sub-μm scale

In the field of new materials development, there are many instances where it is necessary to determine absolute values of thermal parameters. Quantitative mesoscale thermal measurements would benefit the microelectronics industry where thermal properties at the relevant scale differ significantly from the macroscopic value, and reliability depends on understanding mechanisms of heat dissipation at the micrometre level. In addition, quantitative identification of defects in high-conductivity structures made, for example, from chemical vapour deposited (CVD) diamond, will play an important role in achieving consistent performance. Other key areas which would benefit from a reliable version of quantitative thermal microscopy include polymer science, pharmaceuticals and forensic science.

Until recently, the spatial resolution of methods for absolute thermal quantification has been limited by quantities such as the spot size of a laser beam used as the heat source, or by the wavelength of IR radiation used to determine the temperature. The versions of SThM so far described have appropriate resolution, but are not sufficiently quantitative. Nevertheless the resistive thermal probe offers a new way forward, despite uncertainties that result from heat loss from probe to air and uncontrolled variations in probe/sample contact area.

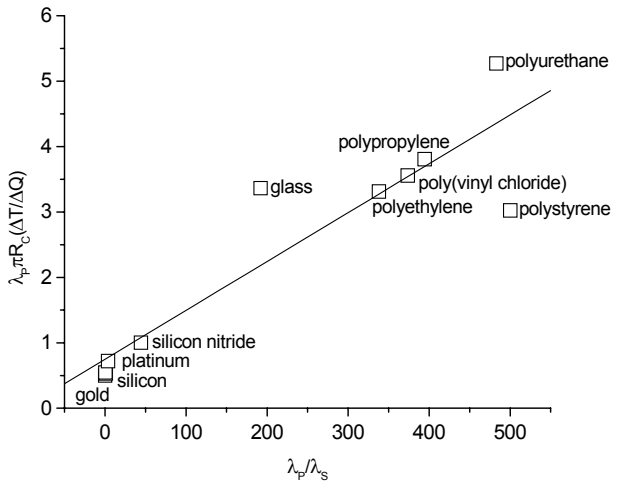

Figure 8. Variation of the reduced heat dissipation at physical contact versus reduced thermal conductivity of various materials normalized to dimensionless units, with linear regression fit: $\Delta T = T_p - T_0$ where T_p is the probe temperature and T_0 is the initial surface temperature; $\Delta Q = Q - Q_0$ where Q is the measured heat dissipation of the thermal probe in the probe–surface contact and Q_0 is the probe heat dissipation before contacting; R_C is the probe–contact radius; λ_p is the thermal conductivity of the thermal probe; λ_s is the thermal conductivity of the sample. (After [49], copyright 2000 Overseas Publishers Association NV, with permission from Gordon and Breach Publishers.)

2.4.1. The dc approach. Recent literature describes two ways of attempting to develop quantitative thermal microscopy—dc and ac. Taking the first of these, Ruiz *et al* [48] developed a relatively simple method for deriving thermal conductivity values from measurements of the heat flux between a Wollaston probe and a sample. They corrected the measured heat flow by subtracting the value measured when the probe was remote from contact. This quantity was then plotted against thermal conductivity for a range of hard materials of known conductivity, giving excellent linearity. An approximate expression for the thermal impedance of a circular contact predicts that this slope is given by the product of the contact radius and the temperature difference $\Delta T = T_p - T_s$ between probe and sample:

$$\Delta Q/\Delta T = k_c \pi r_c \tag{6}$$

where r_c is a contact radius and k_c is thermal conductivity. This equation is valid under the condition $t \gg r_c^2/4\mu$ where t is measurement time at a given data point (about 10^{-2} s) and μ is thermal diffusivity. This procedure was used to determine the thermal conductivity of diamond-like nanocomposite films to a precision of $\pm 15\%$.However, a calibration of this type is necessary each time a new probe is used. Moreover, as discussed earlier, in general the above correction gives only an approximate value of the true probe/sample value of heat flow. Gorbunov *et al* [22, 49] refined the method of Ruiz as follows. Firstly, they verified the linear variation of ΔQ with ΔT (for a given sample) as described by the above equation, by means of experimental data on the change in heat flux as the probe approached the sample surface. They also used a theoretical argument to define the conditions under which this linear behaviour still applies when one takes into account the thermal resistance of the varying air gap as the probe approaches the sample. Finally, they used samples of different known thermal conductivities and plotted the ratio $\Delta Q/\Delta T$ against conductivity (figure 8). Thus, in principle, by means of this type of plot it should be possible to obtain the absolute value of the thermal conductivity of individual regions of an inhomogeneous material. They estimate the thermal conductivity resolution to be ca 0.2 W m^{-1} K^{-1}.

The sensitivity appears to be large enough for quantitative measurements of local thermal conductivity in multicomponent systems to be possible. However, data for low-conductivity polymeric materials (except polyethylene, with the highest thermal conductivity among the polymers studied) are too close to be distinguished with this experimental set-up. A complication with many soft polymer materials is the fact that the effective value of r_c in equation (6) will vary significantly with load and probe radius. In addition, for the thermal conductivity of the sample to dominate the measured value of heat flow, there is a lower limit to the permissible value of contact radius. In the case of a thin-film sample, this contact radius should be kept well below the film thickness, and it may not be possible to satisfy these last two conditions at the same time. Moreover, the linearity of the relation between the heat lost in the probe and sample conductivity is a matter of controversy, both experimentally [43] and theoretically [50]; the conduction loss to the thermal element supports [12] affects the measurement and varies with the thermal conductivity of the sample [43]. This must be taken into account when the relation between the thermal heat flow lost by the probe to the sample and the heat dissipated in the resistive element is established.

2.4.2. The ac approach. Modulation techniques, in principle, have clear advantages over dc methods, for quantitative determinations. Using the third harmonic of the current (the '3-ω method') is an established technique that is often considered to be the optimal measurement method for a system in which the heating element is also used as the temperature measuring element [51, 52]. For example, the 3-ω technique of Cahill [52] uses a single combined heater/thermometer, for use with small (though macroscopic) samples in which a long but thin (100 μm wide) heater can be deposited on the surface of the sample. If a probe of resistance R_p is heated by means of a current $I = I_0 + I_1 \cos(\omega t)$, then the part of the dissipated power (P) that arises from the ac term oscillates at 2ω, since $P = R_p(I_0^2 + I_1^2 + 2I_0 I_1 \cos\omega t + \frac{1}{2} I_1^2 \cos 2\omega t)$. The detected signal depends upon R_p, which varies linearly with temperature, T:

$$R_p = R_0(1 + \alpha T). \tag{7}$$

T will be determined by the dissipated power, P. The relation will depend upon details of various factors such as probe geometry, but T must contain the same frequency terms as P. Thus, where b, c and φ are constants, we have:

$$R_p = R_0 [1 + b\cos(\omega t - \varphi) + c\cos(2\omega t - \varphi)] \tag{8}$$

and the detected temperature signal is determined by $V = I R_p$:

$$V = R_0 \left\{ I_0 + \tfrac{1}{2} I_1 b \cos\varphi + I_1 \cos\omega t + \left(I_0 b + \tfrac{1}{2} I_1 c\right) \times \cos(\omega t - \varphi) + \left(\tfrac{1}{2} I_1 b + I_0 c\right) \cos(2\omega t - \varphi) + \tfrac{1}{2} I_1 c \cos(3\omega t - \varphi) \right\}. \tag{9}$$

Here, we are primarily interested in the terms containing c, since this factor measures how the resistance changes with the 2-ω thermal power only, and not on the current offset I_0. The amplitude of the third-harmonic term depends only on I_1 and c, and is independent of errors based on inhomogeneous temperature distributions in the sample or probe. However, this signal is relatively weak.

Moon *et al* [53] measured the amplitude of the ω term in the voltage signal as a function of temperature modulation amplitude, for polypropylene and sapphire. Fiege *et al* [54] developed a microscale version of the 3-ω method; they used ac heating of a Wollaston wire probe to measure spatial variations in the thermal conductivity of a CVD diamond film. They quote the approximate equation of Cahill [52], as derived from Carslaw and Jaeger [55]:

$$\Delta T = \frac{P}{\pi k_c} [C - \ln(\omega)] \tag{10}$$

where P is the amplitude of the power per unit length of wire and C represents frequency-independent terms involving the thermal diffusivity and the effective diameter of the thermal contact area. Thus, a plot of the temperature signal against the logarithm of frequency has a slope inversely proportional to thermal conductivity:

$$V(3\omega) = I_0 \frac{dR_p}{dT} \frac{P}{4\pi k_c} [C - \ln(\omega)] \sin(3\omega t - \phi) \tag{11}$$

i.e.

$$|V(3\omega)| \propto \frac{1}{k_c}. \tag{12}$$

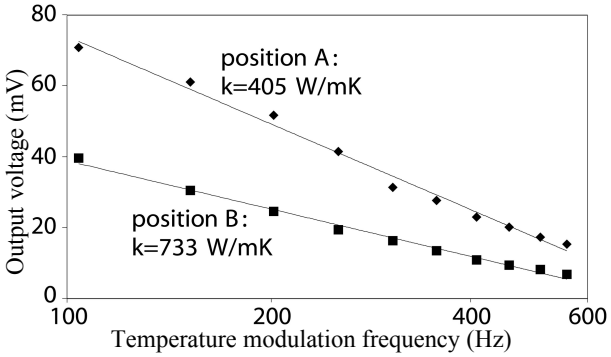

Figure 9. Measurement of thermal conductivity at two locations on a CVD diamond layer; the 3-ω component of the signal voltage is shown as a function of modulation frequency. (After [54], copyright 1999 Institute of Physics Publishing.)

The constant C is eliminated when the 3-ω component of the voltage drop along the probe is plotted against frequency on a logarithmic scale (figure 9). Probe-to-probe variations in the contact area were eliminated by means of reference measurements on standard samples of known thermal conductivities; clearly the roughness and hardness of these reference samples should be similar to those of the sample being investigated.

The plots of temperature variation against log frequency are reasonably straight lines, and enabled Fiege *et al* [54] to derive a value for the thermal conductivity of silver with respect to gold which is within 2% of the correct ratio.

3. Variants of micro-thermal and micro-spectroscopic analysis

In the long-established technique of *thermal analysis*, thermal events, such as a glass–rubber transition or melting of crystalline regions, are detected through measurements of changes in physical properties induced when a temperature ramp is applied to the sample. The measured property may be thermal ('differential thermal analysis', 'differential scanning calorimetry'...) or mechanical ('thermomechanical analysis', 'dynamic mechanical analysis') [56].

However, information derived from all such bulk measurements represents a superposition of information from all of the constituents in the specimen. It was to overcome this limitation that *localized thermal analysis* was developed. Its combination with near-field microscopy constitutes micro-thermal analysis [36, 57, 58]. Once an area has been scanned and images acquired, the probe is moved to selected locations on the surface and a localized thermal analysis measurement is performed at each of these locations. Normally, the active thermal probe, i.e. the same as is used for imaging, is used to provide the temperature ramp, as well as temperature modulation if required, without the use of a sample-heating stage. The chief advantages of this are:

(a) the data are obtained from localized regions chosen from a previously obtained thermal image;
(b) apart from these regions, the rest of the sample is preserved in its original unheated state, avoiding the risk that it will be irreversibly altered (in which case it will be

impossible to achieve the usual objective of microscopical examination, namely the characterization of a material in its as-received state).

The use of a cooling stage is required if the start of the required ramp is below room temperature, for example if low-temperature transitions in a rubber material need to be analysed. It should also be noted that there is one particular advantage of using a temperature stage to heat the whole sample, namely that a conventional sharp AFM probe may then be used to give higher spatial resolution than is currently possible with thermal probes. For example, Reading [59] has shown that in systems where the structure remains invariant with temperature, the use of a normal AFM probe in pulsed force mode [60] can be very effective.

In the next sections, we describe the variants that have so far been put into practice. In the future, it should in principle be possible to develop new imaging modes in which the image contrast is determined by spatial variations in the strength of any of these L-TA signals.

3.1. Localized thermomechanometry

Our starting point is a popular thermal method for use with bulk samples, namely thermomechanical analysis (TMA) in which a controlled force is applied to a probe placed on a specimen. As the temperature is increased, changes in sample length (such as accompany softening during melting) are measured. In this way, thermal expansion coefficients and transition temperatures can be determined, and thermal events detected. If an oscillating load is applied to the specimen, it is possible to monitor the mechanical modulus and damping of the sample as a function of temperature. This technique is known as *dynamic mechanical analysis* (DMA) [56]. Here, the thermal transitions are revealed with very high sensitivity through changes in the real and imaginary parts of the elastic modulus.

In the localized version of thermomechanical analysis (L-TMA) [36, 61], the probe is first pressed against a chosen region of the sample, leading to a deflection of the cantilever, with a given initial force. The temperature-calibrated probe is then heated so as to apply an upward and downward temperature ramp, and its deflection along the z-axis (perpendicular to the sample surface) is recorded. The force feedback mechanism needed for imaging is normally disabled during the experiment, otherwise the z-actuator motion would drive the tip through the specimen as it softens. If the material undergoes a phase transition, its mechanical properties vary (softening), so that the tip will indent the sample and the cantilever deflection will change. In addition to the localized calorimetry, this change in deflection is monitored using the microscope z-axis displacement detection system. Hence, monitoring of the cantilever deflection permits the detection of phase transitions. Because of the small size of the heating element and of the amount of material involved, heating and cooling may be very rapid; the thermal time constant involved is estimated at a few microseconds. The fastest ramp rate that is presently achieved is 1400 °C min^{-1}, as limited by the computer processing time involved when setting the temperature, digitizing and reading in the data.

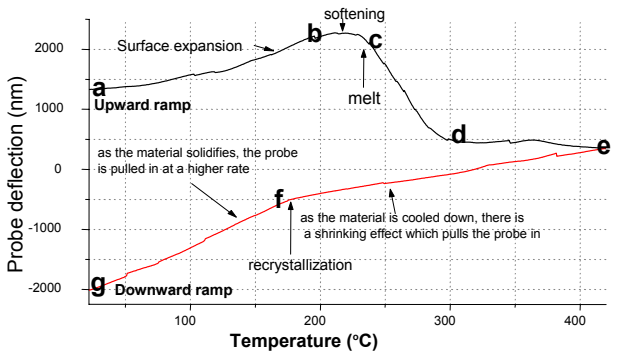

Figure 10. Localized thermomechanical analysis traces recorded with a Wollaston wire thermal probe on PET. Measurements were performed with an initial applied force of 10 μN and a temperature ramp rate of 8 °C s^{-1}. (After [62], copyright 2000 American Vacuum Society.)

Figure 10 shows localized TMA data from one region, consisting of PET, which formed part of a composite sample. The probe in contact with the polymer is deflected as its temperature is ramped up and down. As the material under the probe is heated it expands, deflecting the probe upward (ab); the PET then softens leading to plastic deformation under the pressing probe (bc); it then melts (at between 230 and 260 °C, as confirmed by conventional differential scanning calorimetry) and the tip of the probe sinks into the material (cd) and (de); on cooling, material further away from the surface solidifies and shrinks, so that capillary forces within the still molten material pull the probe further downwards (ef); as material closer to the tip then solidifies, further shrinking occurs, and the probe is pulled in at a higher rate (fg). Tian *et al* [63] have shown that it is possible to detect the melting of an ultra-thin single-crystal film of polyethylene, of a thickness of 11 nm as confirmed by AFM, and it is interesting that direct determination of their melting point may now be performed using L-TA (figure 11(a)). Such measurements are likely to be of value in the studies of polymer crystallization (until recently, it was necessary to work with collected samples using bulk thermal analysis techniques).

3.2. Localized calorimetry

Another long-established group of bulk thermal analysis methods are those that rely on measurements of heat flow. These include differential thermal analysis (DTA) and differential scanning calorimetry (DSC), in which the signal is the measured temperature difference between the sample and a reference. A powerful new development is modulated-temperature DSC (M-T DSC), first described in 1992 when Reading and co-workers introduced a temperature modulation combined with a deconvolution of the resulting data [65, 66]. Here, a cyclic heat flow signal picks out the reversible component of the heat capacity, associated principally with molecular vibrations. The underlying non-cyclic component measurement detects endotherms and exotherms associated with kinetically-controlled processes.

The localized version of DTA [29, 30, 36] is generally used in combination with L-TMA, and the signals obtained simultaneously as the current in both sensing and reference probes is raised as a function of time. An integral control

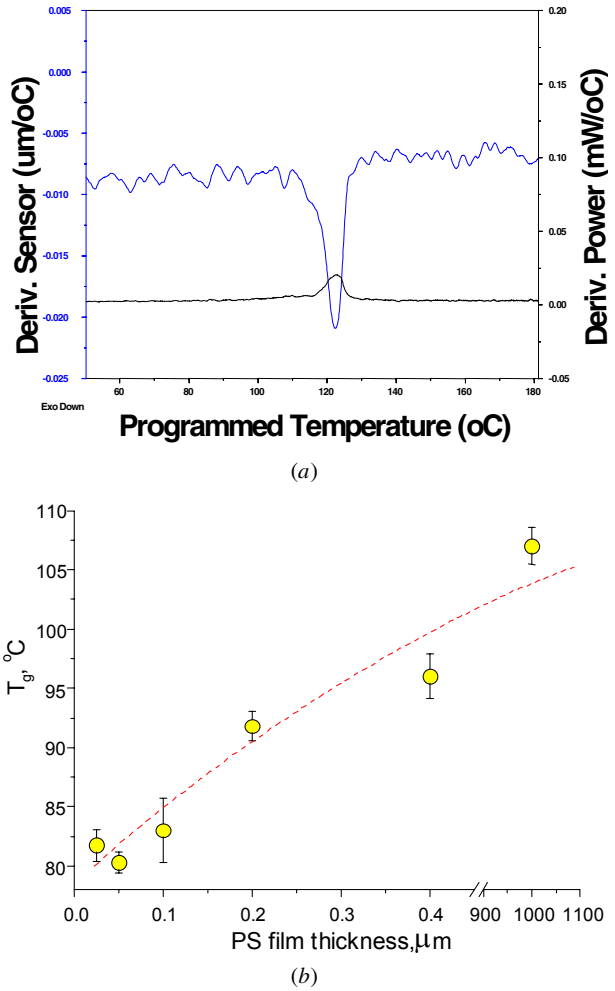

Figure 11. Localized thermal analysis of thin-film samples. (*a*) L-TA performed at the centre of a polyethylene single crystal grown from a xylene solution and deposited on freshly cleaved mica. A melting temperature of ca 123 °C is detected. (After [63], copyright 2001 M-W Tian, J Loos and H Fischer.) (*b*) Variation of T_g for PS with film thickness spin-coated onto silicon, as determined by localized calorimetric analysis. (After [64], copyright 2000 Institute of Physics Publishing.)

feedback may be used to maintain the dc temperature of the sample probe at the value set by the reference probe. In addition, an alternating current is injected into the two probes to produce ac heating. The frequency of the ac signal is higher than the bandwidth of the feedback, which is usually set at 1 kHz, and the current used is such that a temperature oscillation of about one degree amplitude is obtained. The measurement is carried out in a differential configuration in conjunction with a reference probe that is normally suspended in air, though as described by Gorbunov *et al* [64] variations in heat dissipation of less than a microwatt can be detected if the reference probe is made to contact a reference material of similar thermal conductivity to that of the sample. As in any macroscopic DSC measurement, the temperature ramp will in general produce variations in the thermal conductivity and heat capacity of the sample, which may also undergo local phase changes. These variations affect the heat flow out of the probe, and thus the difference in electrical power supplied to the sample and reference probes. In some cases [64], the observed response arises mainly from elastic variations in the tip/sample contact area, as the sample moves from the glassy to the rubbery state. The differences in heat flow are reflected in the measured variations in three signals—the amplitude of the differential underlying (dc) signal, and the phase and amplitude of the dynamic signal as measured through a lock-in circuit. For convenience the method may be termed localized calorimetry (L-CA), although strictly speaking, the term 'L-DTA' should be used rather than 'calorimetry', since the present system is not quantitative in measuring transition enthalpies. Although the probe only senses a small volume (a few cubic micrometres), the sample's mass is unknown, so that at present the measurements are quantitative only in terms of identifying transition temperatures. This is often sufficient for characterization purposes, and semi-quantitative information can be obtained by comparing different areas of the same sample.

Thus, when L-TMA is combined with L-CA, four signals can be measured and displayed: the sensor height position, the differential dc power required to change the probe temperature, and the differential ac power and phase. The L-TMA curve often serves as the primary means of identifying transition temperatures, whereas the accompanying calorimetric response helps to distinguish between melting, crystallization and glass transition phenomena. Melting of the sample is seen as a step change in the power required to heat the probe, whereas glass transitions are seen as a change in slope of the curve. It is therefore convenient to plot the L-CA signals as their first-order derivatives with respect to time or temperature. Several of the figures in section 4 illustrate these points (see, for example, figure 20). The L-CA and L-TMA measurements may be carried out at a heating rate of 10 °C s^{-1}, so that the sequence of measurements can take only a few minutes. Such high heating rates allow a large number of (small) samples to be examined very quickly. It should be noted also that for recording the modulated L-CA signal, the third-harmonic detection method in principle will give clear advantages, just as with ac imaging as discussed earlier. Häßler and zur Mühlen [67] give an example of how the modulated signal is especially useful for a study of phase changes for which a small amount of heat produces a large change in heat capacity.

3.3. Dynamic localized thermomechanical analysis

The well-known technique of technique of *dynamic* thermomechanical analysis [56] involves mechanical modulation (the term 'dynamic' is often used to indicate a change in mechanical force, usually in a cyclic sense). The thermal transitions are revealed with very high sensitivity through changes in the real and imaginary parts of the elastic modulus. We recall that in SThEM, an imposed localized temperature modulation is used to generate thermal expansion, which in turn produces thermomechanical modulation that is used to generate image contrast. In dynamic L-TMA, the modulated stress is applied directly, and accompanied by a localized temperature ramp as used in other forms of L-TA [47].

In order to avoid the spurious lateral force signal that can result from friction, the modulation is applied to the sample *in the plane* of its surface (along the direction in which the probe

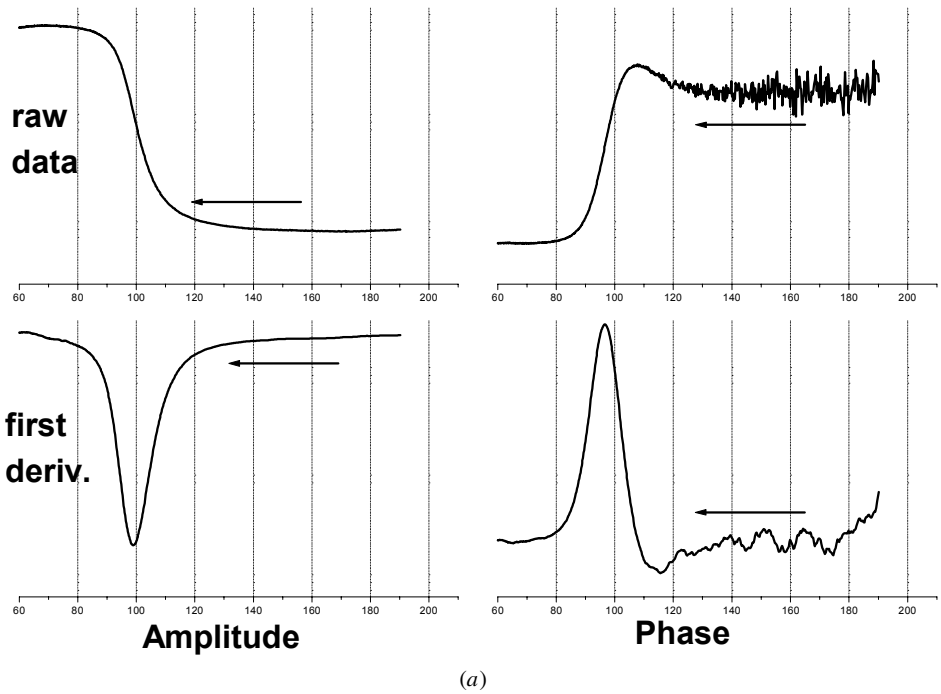

(*a*)

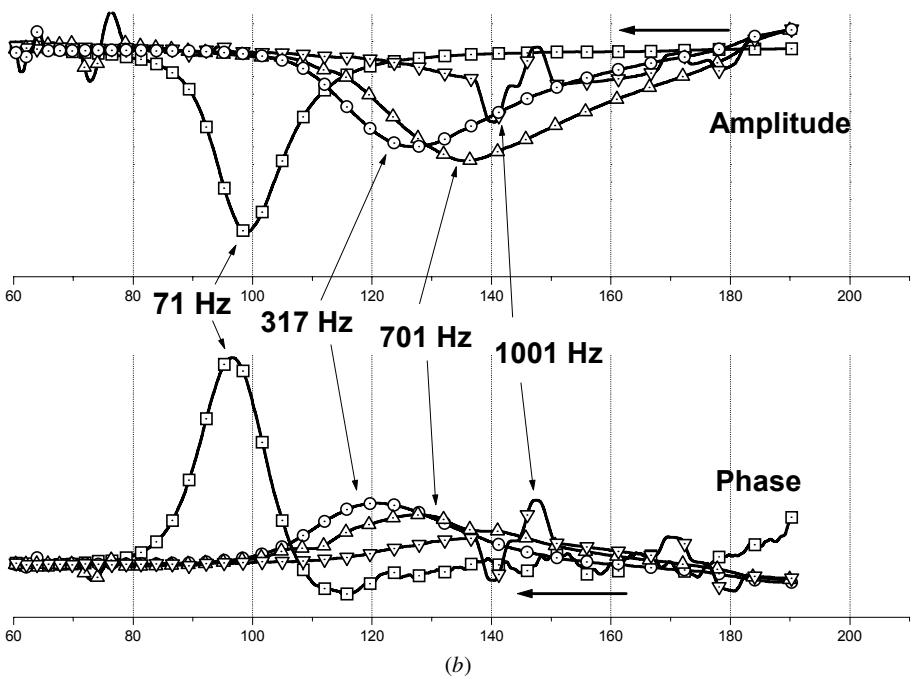

(*b*)

Figure 12. Localized dynamic mechanical analysis. (*a*) Detection of glass transition of polystyrene during cooling. Signal: ac component of lateral force, in response to an applied 71 Hz lateral modulation of the sample position. (*b*) T_g of polystyrene—frequency effect. Signal: as (*a*), but at the four different modulation frequencies shown (□, 71 Hz; ○, 317 Hz; △, 701 Hz; ▽, 1001 Hz). A significant frequency dependence in T_g is seen. This conclusion does not depend upon which feature of the curves is used as the indication of T_g; here we show the first derivative of the amplitude and phase signals. (After [47], copyright 2000 Royal Microscopical Society.)

is stiffest; this is denoted by x, and the normal direction by z). The signals measured are as follows:

- sample scanner; z-position (dc). For a given cantilever stiffness, this determines the normal force ('z-force'). In general, as with other forms of localized mechanometry, force feedback was not used during data acquisition;
- lateral force (dc, along x);
- ac lateral force signal along x (amplitude);
- ac lateral force signal along x (phase).

In experiments on dynamic L-TMA, we have detected the glass transition of the near-surface region of a polystyrene (PS) sample, and this shows a significant variation with frequency (figure 12). Also, the amplitude or phase signal may be used to obtain image contrast that is not related to topography and does not appear in dc images.

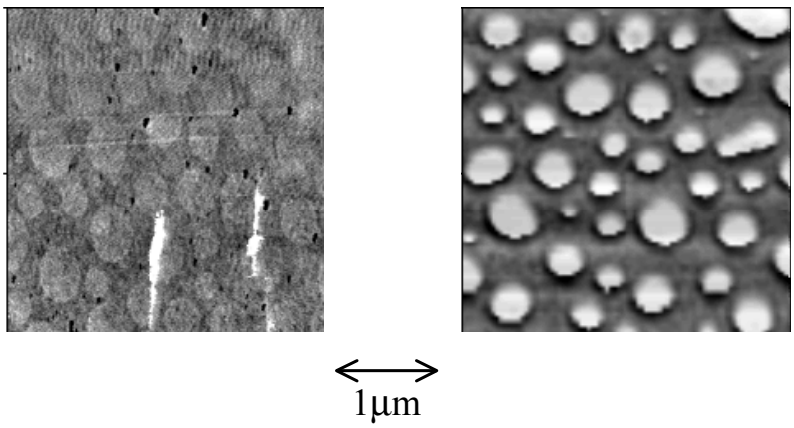

Figure 13. Pulsed force mode imaging with localized heating, using a micro-machined thermal probe. A phase-separated polystyrene/poly(methyl methacrylate) blend is imaged at two different tip temperatures: (*a*) 30 °C and (*b*) 150 °C. With the 150 °C tip temperature, the occluded phase (bright) gives a higher pull-off force, so that this phase is identified as polystyrene. (After [58], copyright 2001 Wiley-VCH.)

3.4. Localized thermo-rheometry

In principle, it is possible to discriminate between different chemical constituents by measuring how their rheological and thermodynamic properties vary with temperature. To achieve this with sub-nanometre spatial resolution promises to provide an attractive mode of micro-thermal analysis. A recently-developed form of intermittent contact AFM is known as pulsed force mode [60]. Here, the image contrast reflects variations in local *adhesion* (or more precisely, 'pull-off force'), as well as in elastic properties. A normal AFM tip is driven into the sample surface and then retracted, at a frequency in the range 0.1–2 kHz, and the force as a function of tip height is measured as a 'force curve', at each point on the spatial scan. Typically, in order to reduce acquisition time and memory requirement, only four points on each of these curves are digitized and recorded, including the pull-off force that is needed to separate the tip from the surface. The values of signals determining the contrast of the pull-off image and the elasticity image are derived from the differences between values of the relevant data points, taken in pairs. The value of this approach does not rely upon quantitative determination of values of thermodynamic parameters such as work of adhesion—indeed, the dependence of pull-off force on elastic and rheological deformation, as well as forces of adhesion, is a complex topic [68]. Pulsed force microscopy (PFM) has been used to study how the properties of several phase-separated segmented polyurethane elastomers, and of blends of polystyrene and poly(methyl)methacrylate (PS/PMMA), change *as a function of temperature* [69]. Since the Wollaston thermal probe is not suitable for PFM, a heating stage was used to vary the temperature of the whole sample, and there was no provision for thermal imaging or micro-thermal analysis.

Recently, the use of the micro-machined bow-tie thermal probes mentioned earlier has allowed this limitation to be overcome, in that the heating may be *localized* as in other forms of micro-thermal analysis. Thus, in principle, the experiments can be performed much more quickly and easily over the same area, the chances of the thermal treatment altering the sample are greatly reduced, and L-CA or L-TMA experiments can be performed to confirm any identification. Work with probes designed to make pits in a polymer coating as a means of data storage [70] indicates that the areas affected by such local experiments may be made as small as 20 nm across. Figure 13 shows high-resolution PFM images of a phase-separated PS/PMMA blend; at elevated temperatures the pull-off force for the PS increases dramatically before any change occurs for the PMMA. Quantitative confirmatory data in the form of pull-off as a function of temperature, for homogeneous samples of PS and PMMA, are presented elsewhere [58]. They confirm that sharp increases in pull-off are observed at specific temperatures, reflecting changes in the viscoelastic responses of each of the two polymers.

Specifically designed probes of this type could also be used in other imaging modes that are sensitive to local mechanical properties, such as phase imaging. In this way, it will be possible to visualize and identify chemical components at a spatial resolution comparable with that of conventional AFM.

3.5. Localized gas chromatography-mass spectrometry

One further capability that has recently been developed is localized evolved gas analysis with mass spectrometry (MS) and gas chromatography-mass spectrometry (GC-MS). The aim is to expand the scope of micro-thermal analysis to include localized chemical analysis of individual domains, features or contaminants [58, 71]. The Wollaston probe is placed on a point of interest within an image and then rapidly heated to 600–800 °C, at which temperature constituents of many types of sample will volatilize or pyrolyse. The resulting plume of evolved gas species is trapped by suction into a tube packed with suitable sorbent, placed close to the thermal probe (figure 14). The sorbent tube is then placed in a thermal desorption unit for analysis of the trapped volatiles by thermal desorption–GC-MS, in order to separate and identify the evolved gases. Figure 15 demonstrates the detection of styrene monomer resulting from the pyrolysis of a small (10×10 μm square) area of polystyrene.

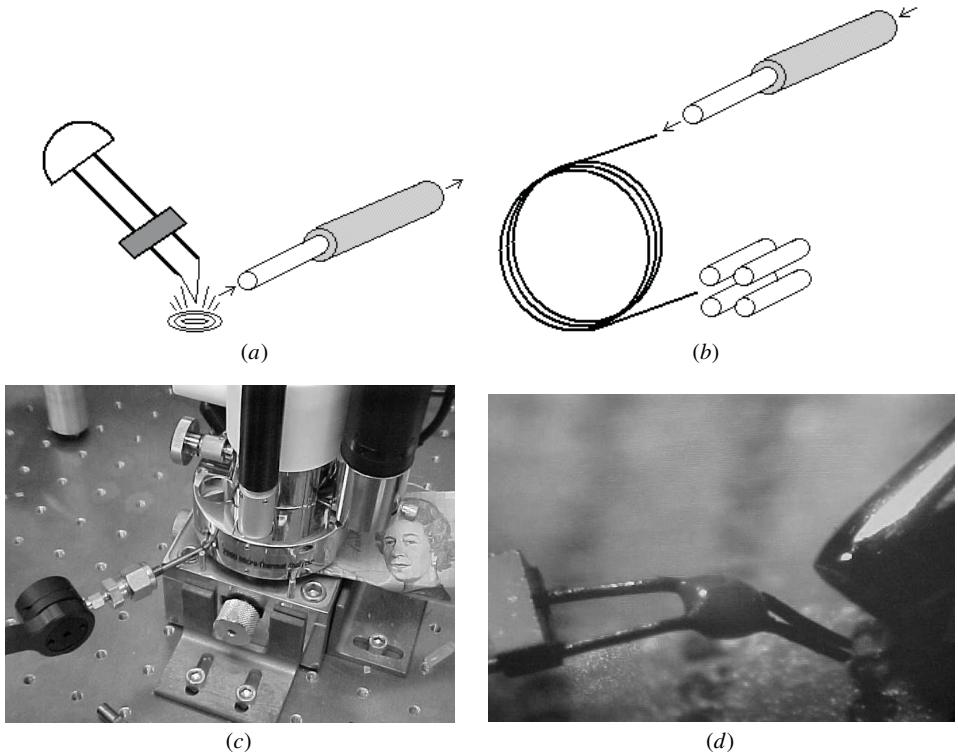

Figure 14. Localized evolved gas analysis with mass spectrometry and gas chromatography-mass spectrometry: (*a*) sampling; (*b*) analysis; (*c*) microscope; (*d*) probe and sorbent tube. (After [72], copyright 2001 D M Price.)

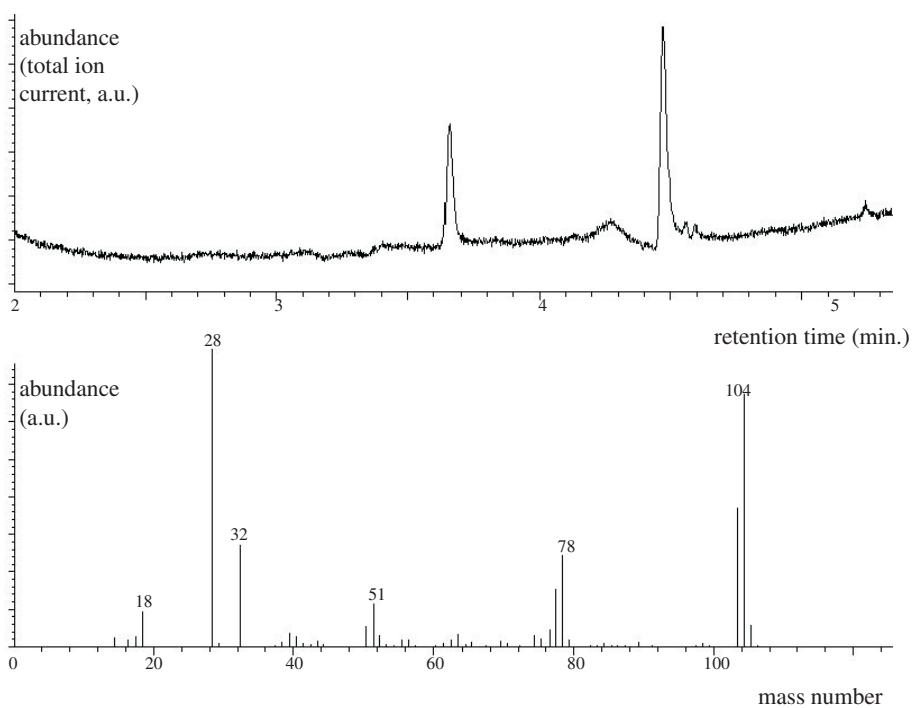

Figure 15. GC-MS data: (*a*) total ion chromatogram of gases evolved from a pyrolysis crater on a polystyrene bead; (*b*) mass spectrum of peak at retention time of 4.5 min. (After [36], copyright 1999, with permission from Elsevier Science.)

Alternatively, mass spectroscopy by itself can be used, if speed of analysis is important; a fine capillary transfer line is placed near the probe and led directly to the ion source of the mass spectrometer. It is also possible to perform thermally assisted nano-sampling [57]. Here, material is extracted from the surface of a specimen by using the heated tip to soften a region and then pulling the tip away as it is cooling, in order to leave a small quantity adhered to the probe. This could then be removed or dissolved from the tip, and qualitatively and quantitatively analysed *in situ* by micro-thermogravimetric

analysis. The extracted material could also be subjected to a number of forms of analysis, including nuclear magnetic resonance spectroscopy or size exclusion chromatography.

3.6. Near-field photothermal infrared spectroscopy

One application of the near-field thermal probe is to achieve chemical resolution combined with sub-wavelength spatial imaging, by detecting *photothermal* signals. Photothermal spectroscopy directly measures infrared absorption by sensing absorption-induced heating of the sample, and we may use the probe to detect the resultant temperature rise as a function of wavelength and of location on the sample surface.

In conventional photothermal spectroscopy [73], a chopped laser beam is scanned across a surface giving rise to an evanescent thermal wave, whose wavelength determines the spatial resolution. The resulting IR radiation, reflected or transmitted, is detected. Typical frequencies are in the region of tens of kHz leading to a spatial resolution (polymers) of tens of micrometres. Photothermal methods [74] are especially well suited to the study of small volumes of material, where the temperature rise for a given input power will be greater. They may be used on a broad range of types of material including thin films and powders, and have depth-profiling capability; if the optical beam intensity is modulated, then variation of the modulation frequency may be used to control the depth below the surface that is being sampled, thanks to the variation with frequency of the attenuation depth of thermal waves.

A version of photothermal microscopy/spectroscopy whose spatial resolution is not subject to the diffraction limit will have clear advantages. Various SPM techniques have been used for the photothermal characterization of solids and thin films [75–77]; for a review, see [78]. Anderson [79] has recently shown that normal AFM probes may be used to obtain photothermal deflection signals, when a sample is exposed to the beam from the hot ceramic source of an FT-IR spectrometer. The AFM tip was used to record the deflection signal resulting from the consequent thermal expansion of the sample surface (compare, for example, the thermal expansion microscopy techniques summarized earlier). This signal has the characteristic form of an FT-IR interferogram, although at the time of writing the corresponding deconvoluted spectra had not yet been published. In addition, it has been shown that the near-field thermal probe, in passive (temperature-sensing) mode, may be used to obtain photothermal spectra of polymers. This offers a new approach to localized IR spectroscopy or infrared micro-spectroscopy.

The dispersive approach. Recently, Stranick *et al* [80] have described an infrared near-field scanning optical microscope that uses absorption as the contrast mechanism. Spectra were recorded using IR laser radiation of wavelength 2.2–4.5 μm. To cover a wider bandwidth, Bozec *et al* [81] have recently made some preliminary photothermal measurements with the Wollaston probe, using an optical parametric generator (OPG) to provide a high-power source, tuneable in the mid-IR from 0.74–18 μm. Figure 16 shows the *C–H* stretching region in polypropylene between ∼2800 and 3000 cm^{-1}. The OPG wavelength was scanned over the region of interest with a resolution of 4 cm^{-1}. We see that the *C–H* band in polypropylene may be clearly resolved, and conclude that it is possible to record spectra by this means. A signal-to-noise ratio of 5 to 1 was achieved for a band of 4 cm^{-1}, after 16 co-additions.

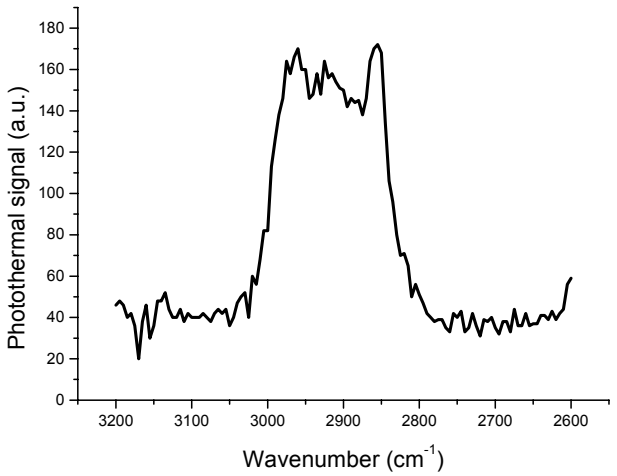

Figure 16. Localized dispersive photothermal spectroscopy. The *C–H* stretch band of polypropylene as detected by differential measurements, using an OPG as an infrared source and a near-field thermal probe to measure temperature. (After [81], copyright 2001 L Bozec *et al*.)

The FT-IR approach. Hammiche *et al* [82] have described the use of the same probe, again operated as a thermometer, to record FT-IR absorption spectra. Sample and probe are fitted inside the chamber of an FT-IR spectrometer, which is operated in the normal way except that its detector is not used. The probe is brought into gentle contact with the chosen region of the sample, and both are exposed to the light beam whose intensity modulation is determined by the motion of the interferometer mirror. As in the dispersive approach, the signal from the probe measures the temperature rise resulting from absorption of electromagnetic energy. However, when an intensity-modulated beam supplied by a normal FT-IR spectrometer is used, the measured temperature fluctuates accordingly. This 'interferogram' signal is amplified, digitized, and fed into the external input of the same spectrometer, and converted into a spectrum by means of a Fourier transform algorithm.

Absorption spectra have thus been obtained for a number of polymers. Data from successive interferograms are averaged and after a few such co-additions, spectral peaks become clearly differentiated. Prominent absorption peaks are clearly resolved and, as shown in figure 17, they correlate well with those contained in a conventional ATR spectra obtained from the same polymer. The technique has been extended to the analysis of real-world industrial samples, both solid (fungicides in a fine powder form) and liquid (surfactants in liquid solution form). The method has also been used to study bilayers, and it is possible to detect a buried layer of PS covered by polyisobutylene (PIB) of a thickness up to at least 15 μm. From the variation of peak height with layer thickness, it was possible to derive a value of the thermal diffusion length in PIB (13.8 ± 0.9 μm at a frequency of 100 Hz).

Prospects for high spatial resolution. In photothermal imaging, the signal amplitude will depend on the thermal

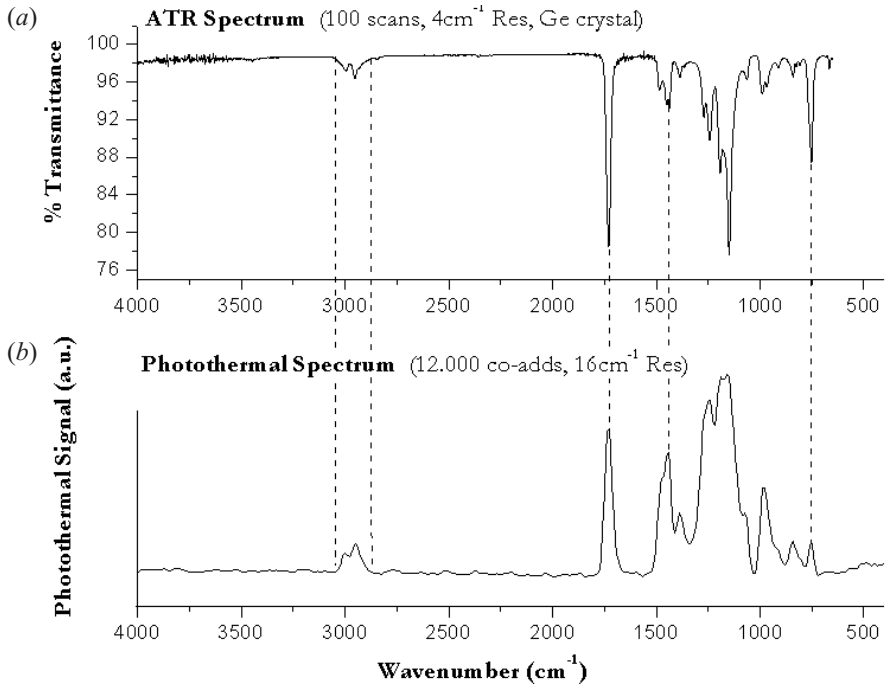

Figure 17. Localized photothermal FT-IR spectroscopy: (*a*) spectrum of PMMA obtained using conventional ATR FT-IR spectroscopy; (*b*) the corresponding photothermal spectrum obtained using the near-field thermal probe. (After [32].)

properties of the materials involved, as well as the optical properties of the absorbing regions. An example of a theoretical estimate of spatial resolution in near-field photothermal FT-IR microscopy, based on the 3D temperature distribution such as might be obtained when an inhomogeneous polymer sample is to be examined in practice and neglecting the effect of modulation, has been given by Hammiche *et al* [82] (figure 18). The sharp temperature drop shown, as the probe crosses the boundary between a strongly-absorbing to a non-absorbing region, suggests a value of 0.1 μm as an upper limit to the spatial resolution in this example. This opens the way to IR microscopy at a spatial resolution well below the diffraction limit of IR radiation, ultimately at a scale of 20–30 nm.

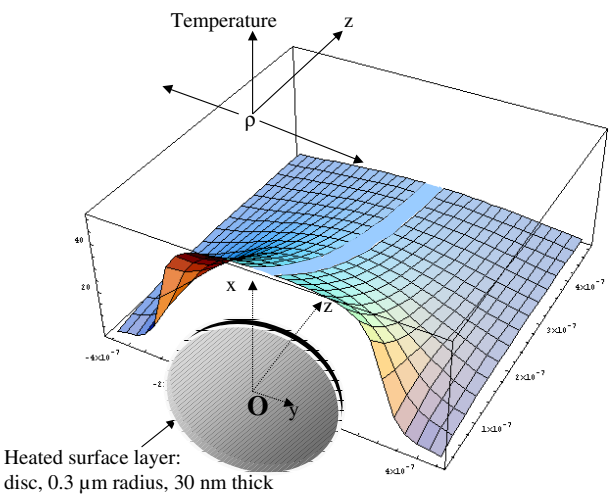

Figure 18. Effect of absorbed IR energy within near-surface region (a thin disc-shaped inhomogeneity at the sample surface, of radius $\rho_0 = 0.3$ μm and thickness $z_s = 30$ nm, in the xy plane), uniform heat flux 1400 Wm^{-2} within a 200 nm wide band of the IR spectrum. The resulting excess temperature distribution is shown in three dimensions as a function of radial distance ρ and depth z, for a thermal conductivity of 0.15 Wm^{-1} K^{-1} and an absorption coefficient of 0.4 μm^{-1}.
As we move outwards from the centre of the disc-shaped inhomogeneity, the excess surface temperature within the central region is constant to within approximately 20% until we reach a distance equal to 75% of the disc radius. The excess temperature then falls sharply, until at a distance equal to 110% of the disc radius it has fallen to 10% of that of the centre of the disc. (After [82], copyright 1999 The Society for Applied Spectroscopy.)

4. Applications

4.1. Distinguishing different constituents of a heterogeneous material: various examples

We now turn to various applications of micro-thermal analysis that have been described in the literature to date, beginning with the fact that in many cases, different constituents of a heterogeneous sample cannot be unambiguously distinguished solely from the thermal image. Generally, this is because the image contrast is unavoidably affected by sample roughness as well as thermal properties, and there is as yet no reliable way of deconvoluting the two effects (though as mentioned later, some progress in this direction is being made). However, it is always possible to use the image to choose individual points at which thermal profiles are to be obtained, and we now give examples of studies in which a thermal profile, such as the localized thermomechanical scan, allows a clear distinction to be made between individual components of a composite sample.

4.1.1. A polymer blend. Figure 19(*a*) shows the dc thermal image of a two-component blend of partially hydrolysed poly(vinyl acetate) and poly(vinyl butyrate). From M-T DSC

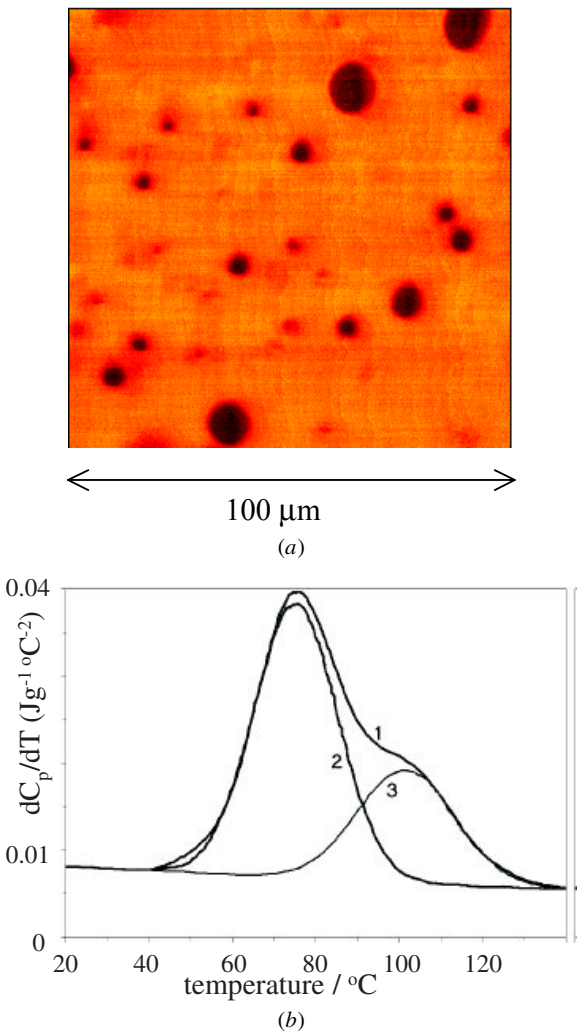

Figure 19. Localized analysis of an inhomogeneous sample. (*a*) The dc thermal image of a two-component polmer blend: dark areas represent regions of low thermal conductivity. (After [83], copyright 1999 Akadémiai Kiadó Rt.) (*b*) First derivative of heat capacity with respect to temperature for the blend shown in (*a*). (After [83].) The procedure of Song *et al* [84] was used to separate the raw response of the sample (curve 1) into two peaks (curves 2 and 3) which can be compared with the individual components. The areas under these peaks represent the change in heat capacity of each component as it devitrifies (ΔC_p), and the peak positions identify the glass–rubber transition temperature.

measurements of the bulk material (figure 19(*b*)), the blend is known to be immiscible. The M-T DSC data also give the composition of the blend (70:30 by weight), but do not indicate the spatial distribution of the phases. In the image, dark regions of low thermal conductivity can be seen within a matrix of higher thermal conductivity material. From the compositional analysis determined by M-T DSC, it would be expected that the dark regions are the minority, higher T_g component. This was confirmed by L-TMA measurements [83], where observed step changes in the first derivative of the power applied to the probe were able to resolve the spatial variations in the glass transition temperature.

4.1.2. Phase separation. Miscible polymer blends usually form metastable systems. Diffuse interfaces are important in adhesion, welding, crack healing and film integration; when mutual diffusion is possible, then with the help of controlled phase separation, a range of performance characteristics can be achieved, leading to a large number of potentially useful and different products. Since most of the useful polymer blends are immiscible, it is important to be able to study phase separation processes. This has for some time been possible with the help of scattering and solid-state nuclear magnetic resonance techniques. The former gives information about apparent macromolecular diffusion coefficients, and changes in phase structure with time; the latter reveals qualitative detail on the variation of concentration with time, and also on diffusion coefficients when used in combination with optical microscopy. However, it is difficult to obtain information thereby on how the distributions of concentration and domain size vary with time, or on the early stages of spinoidal phase separation. Moreover, ternary polymer blends can decompose into more than two phases, in which case the scattering technique loses its usefulness.

Many questions arise in connection with the physical processes involved. For instance, it may be important to know the conditions under which phase separation occurs, either on a microscale, by segregation at interfaces so as to give interface thickness ('diffuse interface development'), or by nucleation and domain growth (from an initially miscible state). In this connection, Pollock *et al* [31] used SThM to carry out some preliminary work on both spinodal and binodal processes in the case of the poly(vinyl methyl ether)/polystyrene (PVME/PS) system. They obtained a series of constant temperature (35 °C) thermal images obtained for a PVME/PS (40/60% weight ratio) blend, miscible when initially cast onto a glass slip, but then subjected to an annealing temperature of 105 °C for increasing annealing times. Binodal decomposition in the form of a nucleation and growth process was clearly identifiable; PS nuclei were seen to form and grow within the matrix. Intermediate miscibility blends were also observed, but they disappeared as decomposition led towards complete separation of the phases. The mean dimensions of the segregated regions were observed to grow linearly with time, as is known to be characteristic of the 'diffusion and flow' stage [85] of domain growth.

Once the spatial resolution of SThM has been improved on a routine basis, it will be possible to extend such studies to cover domain distribution during phase separation, for ternary as well as binary blends; segregation at the interface between two principal phases; and the role of blend symmetry or asymmetry in the phase separation process. Fischer [26] has recently described examples of how the thermal probe may be used to achieve controlled phase separation, in the form of the so-called self-stratifying effect in thin films of polymer blends. The experiment achieved controlled surface demixing of a mixed blend while scanning at elevated temperatures. The technique is similar to that used to make pits in a polymer coating as a means of data storage [70]. For example, a polymer blend system (PMMA and a fluorinated polymer), miscible at low temperatures and immiscible at high temperatures, has a glass transition temperature of about 100 °C when in the mixed phase, and two glass transitions at about 78 °C and 105 °C when demixed. The demixing temperature is ca 200 °C. The thermal probe was placed carefully onto the surface and

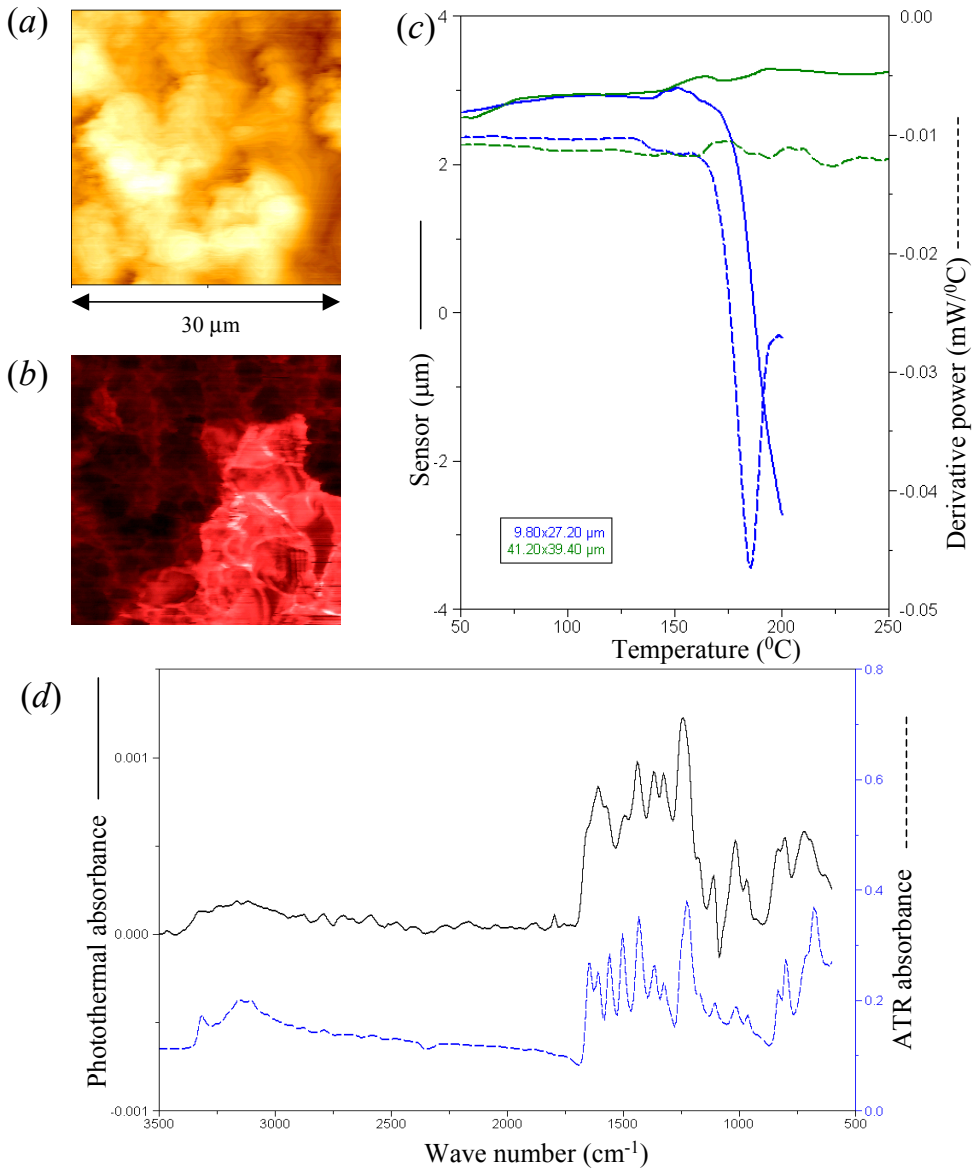

Figure 20. Localized analysis of a pharmaceutical tablet. (*a*) Topographic and (*b*) dc thermal images of a different area of the same paracetamol tablet as was shown in figure 6. (After [86], copyright 1998 Dr A Murray.) (*c*) Two locations on the tablet were examined by L-TA, one from a region of high thermal conductivity (showing bright in the dc thermal image), and one from a low thermal conductivity region. (After [86].) The continuous lines show L-TMA scans, and the dashes show L-CA scans. Scans on the dark areas (blue curves) show melting transitions corresponding to the known melting point of the drug, whereas scans on the bright regions (green curves) showed no transitions over the temperature range studied. The high thermal conductivity inclusions (invisible in the conventional topographic image) are probably composed of an inert filler such as microcrystalline cellulose or calcium carbonate. (*d*) Photothermal absorption spectrum of pure 4-acetamidophenol (solid line) acquired using the thermal probe—the conventional ATR spectrum is shown (dashed line) for comparison. (After [57], copyright 1999 Akadémiai Kiadó Rt.)

then heated to 200 °C, an area of 50 μm by 50 μm was scanned, and the probe was then lifted. Subsequent L-TA data clearly showed a decrease in the glass transition temperature of the scanned region, consistent with an enrichment of the fluorinated component at the surface.

4.1.3. Pharmaceutical applications. Figure 20 shows images of a tablet of paracetamol (4-acetamidophenol), together with the localized TMA data. Despite the roughness revealed by the topographic image, the thermal images indicated that two thermally dissimilar materials are present. The localized spectroscopic data from the same material are also shown. Figures 6(*d*)–(*f*) showed ac thermal images of the same tablet; as the frequency is increased, the second component disappears from view, suggesting that it is buried within the lower thermal conductivity matrix.

As another example, we mention the work of Craig and colleagues [87] on the characterization of controlled release tablets. They have used micro-thermal analysis to differentiate between an active drug (ibuprofen) and an inert matrix (hydroxypropylmethyl cellulose). The significance of this is that clearly the drug must dissolve before being required to be absorbed across biological membranes; the rate of dissolution will thus control the onset and duration

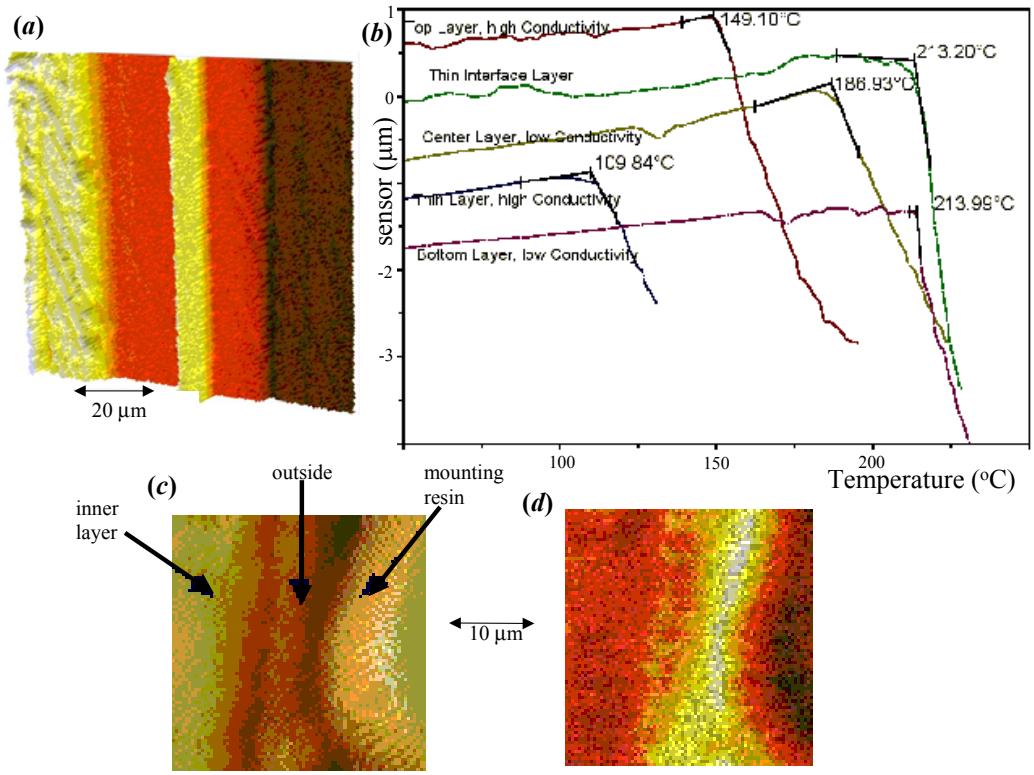

Figure 21. Film cross sections. (*a*), (*b*) Cross section of multilayer packaging film. (After [89], copyright 2000 E zur Mühlen.) In the dc thermal image (*a*), the individual layers can clearly be distinguished by their differences in conductivity, and then identified through their melting temperatures. High-resolution images of the interface reveal the presence of a thin layer between the HDPE layer and the wider adjacent one. The low conductivity area with a width of 20 μm on the right shows the embedding resin and is not part of the multilayer system. In the L-TMA data (*b*), the top curve has been obtained from the outside layer with a high thermal conductivity (i.e. the layer appearing bright at the left of the image in (*a*)); since a melting transition of almost 150 °C is observed, this layer can be assigned to HDPE. The thin interface layer has a thickness of only 2 μm and shows melting above 210 °C, indicating the presence of PA6, while the melting temperature of 187 °C suggests EVOH as material of the next layer. Finally the next two layers of high and low thermal conductivity can be assigned to LDPE and PA6 due to their melting temperatures of 110 °C and 213 °C, respectively. (*c*) Topographic and (*d*) thermal images of the cross section though a sample of PE coated styrene-butadiene rubber film, embedded in an epoxy resin block and cut with a microtome. The mounting resin can be seen on the right of the image and a 5 μm thick surface layer can be seen between the bulk of the film and the resin. (After [58], copyright 2001 Wiley-VCH.)

of activity. This can be controlled through the design of the dosage vehicle, so as to reduce the dosing frequency for example, or to maintain a steady level of active agent in the blood. This group have also studied the distribution of active drug material on surfaces of microspheres used to deliver a variety of drugs including vaccines, hormones and anti-tumour agents [88]. The mechanism of drug release may involve either diffusion or erosion of the microspheres, whose physical structure is therefore of importance. The softening temperature of drug-loaded polylactic acid microspheres has been determined from measurements involving micro-thermal analysis. The softening events revealed by L-TA profiles provided evidence supporting the hypothesis that the active material (drug) is distributed as a deposit on the surface of the microspheres. Although the thermal event noted may simply represent softening rather than an actual glass transition, there is no reason why the method should not remain valid even when this is the case.

4.1.4. Films. If a film a few micrometres in thickness contains buried inclusions, these may often be detected by means of ac thermal imaging. For example, zur Mühlen [89], in a study of a metallic paint film, has shown how dc and low-frequency ac images display sub-surface particles, while high-frequency ac images show only particles present at the surface. A fundamental but controversial topic of great interest is the question of the extent to which the constraining proximity to an interface or a free surface modifies the molecular mobility, and hence the value of the glass transition temperature, of polymer material in thin-film form. This has been investigated by Overney *et al* [1], using force modulation microscopy in conjunction with a heating/cooling stage, to perform scanning friction and shear modulation experiments. Gorbunov *et al* [64], using L-CA, have found that T_g for PS films 25 nm thick is 20 °C below the bulk value (see figure 11(*b*)). The localized thermo-rheometry approach outlined earlier (see figure 13) could have advantages in future studies of this kind involving heterogeneous samples for which the heating/cooling cycle produces irreversible changes structure or morphology.

On a more applied theme, polyethylene (PE), low-density polyethylene (LDPE), medium-density polyethylene (MDPE) and high-density polyethylene (HDPE) are widely used in different food packaging applications in the form of flexible films and laminates for bags, and as semi-rigid and rigid containers as well as in pipe extrusion and injection moulding

of different items. Using classical techniques it is difficult to identify the grade of polymer used, particularly in the case of a commercial film. In two studies [61, 89], micro-thermal analysis has been used to 'fingerprint' the polymer type, and to identify the interface between layers, even in cases where there is no obvious change in image contrast. The data show excellent reproducibility, and the sequence of measurements can be conducted in a matter of a few minutes because of the high heating rates that are employed. In addition, variations of melting within a layer of known composition reveal information about important properties of crystallinity and/or orientation of the polymer.

In the study by Price *et al* [61], different layers were identified as HDPE, EVOH, MDPE, and an interface between the LDPE and HDPE layers. Figure 21 is reproduced from a report by zur Mühlen [89] and shows an example of the cross section of such a film. Recent micro-thermal analysis of a perforated rubber film, used in medical and sanitary applications, provides another example of the characterization of a film material [58]. A 5 μm thick surface layer was revealed in the topographic and thermal images, and its melting point, as measured by L-TA, indicated that this layer is composed of PE. The bulk material was analysed by micro-GC-MS and the results suggest that this polymer is synthetic poly(butadiene-styrene) rubber rather than natural rubber.

As a last example of the use of micro-thermal analysis to identify spatial distribution, we mention [90] a study of the morphology of a welded joint between two polymers, produced by heating a wire embedded in one polymer just below its surface while in contact with the second material. The temperature rise at the interface is just enough to fuse the two surfaces together. However, too much heat can make the material degrade through cross-linking. L-TMA was performed at different points across the region around the heater wire, in order to measure the softening temperature of the polymer. The data showed that as one moves further from the heater, the softening temperature falls, then rises again, while polymer lying on the weld line has a softening temperature above 400 °C. It was speculated that the mechanical vibration brought about by ac heating of the wire may have provided a localized source of heat along the weld line itself.

4.2. *Polymorphic forms of polymers: thermal history*

The identification of polymorphism, the existence of a substance in more than one structural form, is becoming increasingly important within the pharmaceutical industry. Here we give examples of the use of micro-thermal analysis in this context.

4.2.1. Amorphous and crystalline forms of a drug material. Micro-thermal analysis has been assessed as a possible means of quality control in the formulation of compressed tablets. To this end, it was necessary to differentiate between amorphous and crystalline regions. Figure 22 shows images of a drug sample, aged amorphous indomethacin, together with L-TMA data [91]. These allowed the growth of crystalline regions to be followed. Scans were taken from regions selected according to their characteristic appearance in the topographic

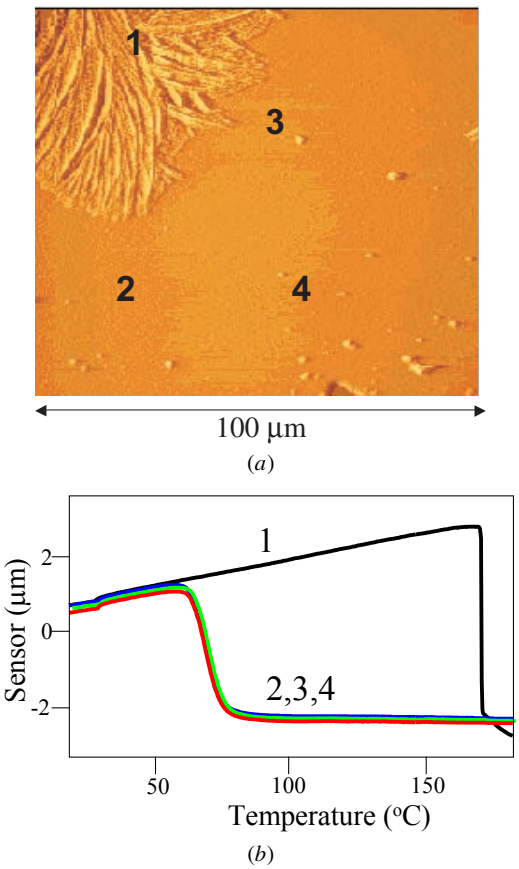

Figure 22. Aged amorphous indomethacin: (*a*) SThM images and (*b*) L-TMA traces allow the growth of crystalline regions in otherwise amorphous drug material to be followed. (Reprinted with permission from [91], copyright 2001 American Chemical Society.)

images, and were compared with scans from samples known to be either amorphous or crystalline. This has important implications for the possible monitoring of the physical stability of pharmaceutical materials. Indeed, such work points to the fact that often the key benefit of micro-thermal analysis will lie in the study of different physical forms of the same material, and not just in distinguishing chemical entities.

4.2.2. Polymorphism of the drug cimetidine. Sanders *et al* [92] have shown that SThM combined with micro-thermal analysis can be successfully employed to distinguish between two polymorphs (types A and B) of the drug cimetidine. SThM imaging showed that a sample consisting of a 50:50 mixture of the polymorphs contains regions of different thermal conductivity. Micro-thermal analysis of pure polymorphic samples demonstrated that the origin of the thermal conductivity contrast lies, at least in part, in the presence of a surface water layer in the case of type A that is not present in type B.

The origin of the differing surface thermal conductivity of the A and B polymorphs of cimetidine is initially unclear, since they display very similar bulk thermal behaviour. Micro-thermal analysis of pure disks of each polymorph allowed elucidation of the contrast mechanism. The most surprising feature of the data seen for polymorph A was an endothermic differential thermal peak seen just above

100 °C. No corresponding transitions were seen in the L-TMA curves, which suggest this feature is not a result of change of polymorphic state or phase. It is seen in neither the bulk thermal analysis of form A nor the micro-thermal analysis of form B. This would suggest that this feature is a result of the increased surface sensitivity of the micro-thermal technique. The endothermic peak is likely to be a result of adsorbed surface water. This postulate has been substantiated by independent contact angle measurements (which show form A to be more hydrophilic than form B) and scanning probe phase-distance data, which also display behaviour indicative of adsorbed water at the surface.

4.2.3. Thermal history of polymers. Quantitative confirmation has been presented [31] to show that the crystallinity of samples of different branched polyethylenes, as measured by M-T DSC, correlates well with the magnitude of the derivative of the localized calorimetric phase signal. Recently, Grandy [93] has performed a detailed μTA study of poly(ethylene terephthalate) with different degrees of crystallinity, exploring the effect of variables including heating rate, probe force, tip geometry, and modulation amplitude and frequency. The areas under the melting peaks correlate well with M-T DSC data obtained from the same samples. Such studies of the occurrence of different polymorphic forms will generally throw light on the thermal history of the polymer involved. For example, Hammiche *et al* [62] have have analysed samples of commercial grade quenched PET using (a) L-TA, and (b) conventional bulk DSC. With L-TMA, different results were found according to whether the sample consisted of the surface of a pellet of the material, the face of a pellet that had been cut in half, and the surface that had been in contact with the holding pan of the DSC instrument. From an analysis of all these differences, it was deduced that the pellet surface was highly crystalline. This was a consequence of the extra forces on the outside of the material during extrusion giving rise to alignment of the polymer molecules at this surface. The surface in contact with the holding pan undergoes only a clear melting transition; it has cooled at such a rate during the DSC experiment that the sample reaches its glass transition temperature at the surface before it can fully recrystallize.

These results show how micro-thermal analysis may be used to characterize inhomogenieties in properties such as crystallinity and consequently, by supplying spatially resolved information, can yield a much more complete characterization than is possible with conventional thermal methods.

4.3. Identification of a contaminant or surface film

Next we mention the use of micro-thermal analysis to detect and analyse very small quantities of material, in addition to the example already discussed (figure 11). As described by Price [94], the dc thermal image in figure 23 shows a PS sheet that was believed to be contaminated with some low molecular weight poly(α-methyl styrene) (PaMS). A region of inhomogeneity was identified in the thermal image across an interface between what appear to be two thermally dissimilar materials. Localized TMA measurements on the top and bottom regions suggest that they are indeed different materials. The glass transitions correspond to the features in bulk M-T DSC results and indicate that the top area is PaMS and the bottom area is PS. Following the TMA measurements, the thermal probe was used to pyrolyse the surface at the same locations. The GC-MS data detected differences in the evolved gases—the mass spectra of the main peaks forming the GC-MS traces are shown also. These confirm that the top region is PaMS (by detecting α-methyl styrene) and the bottom region is PS (by detecting styrene).

In a second example, an image subtraction technique has been used [15] to help characterize a sugar-based film coating on a commercial pharmaceutical tablet. In an attempt to reduce the unwanted extent to which surface topography (roughness) degrades the thermal image, the following technique was used. For each area, two ac thermal images were obtained, one with a high modulation frequency (20 kHz) providing near-surface information, and one at 2 kHz whose image contrast thus sensed thermal properties to a greater depth. The effect of topography was assumed to be similar in the two cases. Thus, the 'differential' thermal image obtained by subtracting the 20 kHz data from the 2 kHz data was expected to be relatively free of topographic degradation. As shown in figure 23, the result did indeed clearly show a distinction in the differential thermal image between coating (upper left of image) and matrix (lower right). In addition, the onset points for softening clearly identified the two regions.

4.4. Biological applications

As an example of how micro-thermal analysis could be of value in the biological field, we mention the possibility of studying plant leaves under metabolically active conditions. If a better understanding could be gained of how pesticides, weedkillers and fertilizers work at the micrometre level, the waste of such active agents could be greatly reduced. Price *et al* [83] have used L-TA to scan part of a leaf from a specimen of *crassula argentea*. All plant leaves are covered by a waxy film which serves to protect the leave and prevent moisture loss from the cells. This is particularly important for cacti and succulents which are adapted to live in arid climates. The melting of the wax layer (ca 1 μm thick) was indicated by the penetration of the probe into the specimen and by an endothermic peak in the derivative power curve. At higher temperatures, it was found that an exothermic process occurred which shifts to a higher temperature with an increase in heating rate, suggesting that it is a kinetically controlled process. The melting of the wax was unaffected by heating rate. In another study, Price *et al* [71] have used AFM combined with localized GC-MS to detect camphor in a nodule of the leaf of the feverfew plant.

Hodges [95] has used SThM to study the structures of *biofilms*, which are formed when bacteria grow in locations such as pipelines and heat transfer equipment. Such studies are relevant to current efforts to find ways of reducing the corrosion that can be produced by sulphate-reducing bacteria on steel surfaces, for example. Figure 24 shows images of a biofilm formed by three weeks' growth of a fresh water bacterium in glucose solution; the structural features are seen much more clearly in the thermal images. This is probably a consequence of differences in film thickness produced by the collapse of the bacteria on dehydration.

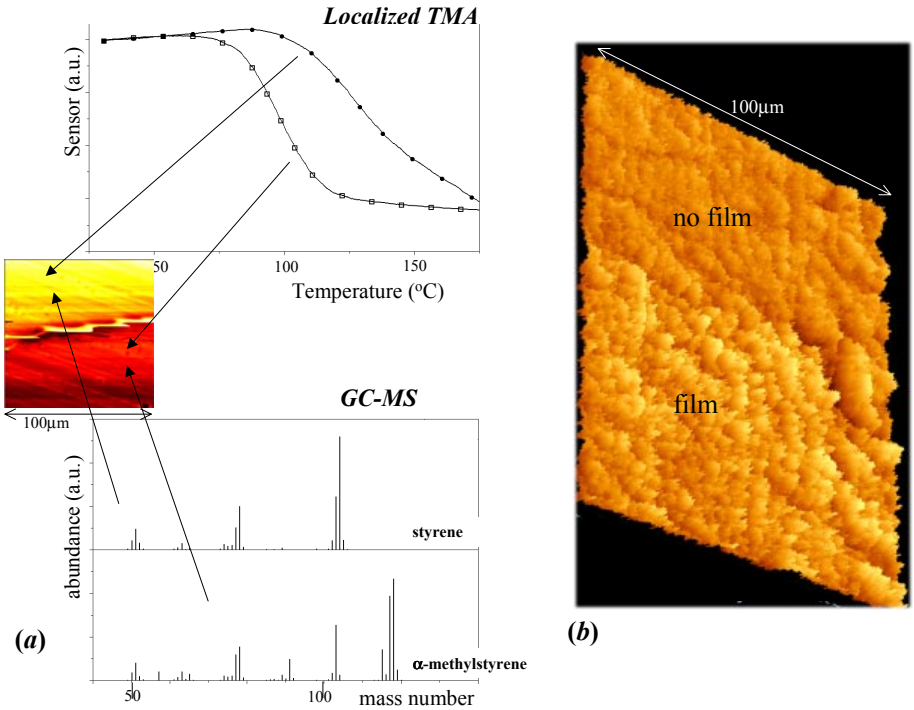

Figure 23. Surface contamination. (*a*) PS sheet believed to be contaminated with some low molecular weight poly(α-methyl styrene) (PaMS). The dc thermal image shows a region of inhomogeneity between two thermally dissimilar materials. The L-TMA measurements on the top and bottom regions reveal the glass transitions corresponding to PS and PaMS. GC-MS traces of the main peaks from the evolved gases show styrene from the top region and α-methyl styrene from the bottom region. (After [94], copyright 2000 D M Price.) (*b*) Sugar-based film coating on a commercial pharmaceutical tablet (ibuprofen). The 'differential' thermal image (with a probe temperature of 60 °C), obtained by subtracting 20 kHz ac image data from 2 kHz ac image data, reduces the unwanted extent to which surface topography (roughness) degrades the image data. (After [15], copyright 2000, with permission from Elsevier Science.)

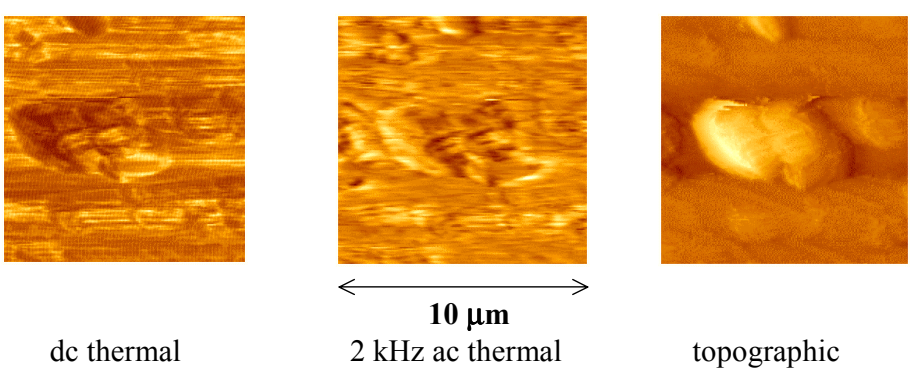

Figure 24. Images of biofilm (10 × 10 μm), formed by three weeks' growth of 'K9' bacterium (origin: Windermere) in glucose solution, with a strength of 5 μg ml^{-1}. (After [95], copyright 1999 C S Hodges.)

4.5. Microelectronics applications

Thermal measurements at the sub-micrometre level are likely to provide key data for the study of irreversible heat flow and failure mechanisms in electronic and optoelectronic devices, as has been discussed by Majumdar whose review [12] gives examples of the use of thermocouple thermal probes to study temperature distributions in field-effect transistors. In a study of integrated circuit interconnects that had suffered electromigration damage, Buck *et al* [96] used the Wollaston probe in temperature mode to detect large voids in metal tracks that were buried beneath a polyimide passivation layer. Recently, micro-thermal analysis has been used to characterize light-emitting diodes and to study thermal cure of dielectric polymers. Figure 25(*a*) shows the topography, dc and 30 kHz ac thermal images of a light-emitting diode [83]. Both thermal images also show marked differences in contrast between the centre of the image and the outside. These differences cannot be attributed to the roughness, and were investigated by performing L-TMA measurements at five different positions on the sample, as shown in the graph. The difference in thermal expansion coefficients of the component parts of the diode is clearly seen. When a different LED was examined, no thermal image contrast was observed, although a similar topography was obtained. L-TMA confirmed that the surface was homogeneous, and further investigation discovered that this component had been coated with a protective layer.

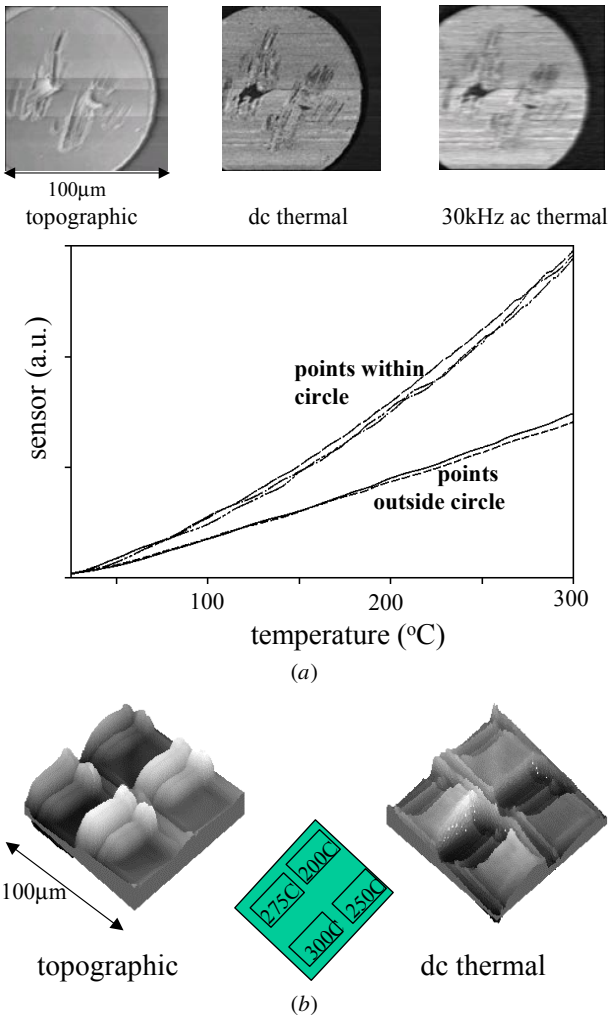

Figure 25. Applications to electronics. (*a*) SThM images of a light-emitting diode; the scratches in the centre of the topographic image are an artefact caused by the removal of a gold contact wire. The L-TMA measurements were taken at five different positions on the same sample, showing differences in thermal expansion coefficient. (After [83], copyright 1999 Akadémiai Kiadó Rt.) (*b*) Thin layer of DVS-bis-BCB, a low thermal conductivity dielectric polymer used for microelectronic applications. The BCB was cured locally at various temperatures in a nitrogen atmosphere, using the thermal probe as a heater (from [97]).

Work at Dow Chemical [97] has included a study of spin-on, low thermal conductivity thin dielectric films, in particular benzocyclobutenes such as 1,3-Bis(2-bicyclo[4.2.0] octa-1,3,5-trien-3-ylthenenyl)-1, 1,3,3-tetramethyl-disiloxane homopolymer (DVS-bis-BCB) which has a very low permittivity, for microelectronics applications. These allow thermally cured, photodefinable (or dry-etch) formulations to be devised, without the need for catalysts and with no volatile by-products. They are easily processed as spin-on oligomer formulations. The thin polymer layer on silicon was imaged after hot plate baking at 125 °C. We see the results of an experiment in which the BCB was further cured locally at four different temperatures in a nitrogen atmosphere, using the thermal probe as a heater (figure 25(*b*)). From the series of dc thermal images it is seen that heat flow generally increases with increasing tip temperature used for curing. However, as seen from the topography images, at these temperatures the load applied by the probe causes some surface damage. In addition, micro-L-TA profiles have been successfully used to study the extent of thermal cure and of ambient on the surface glass transition temperature using the same thermal probe.

4.6. Interfaces and interphases

One of the least understood aspects of the physics and chemistry of polymers is what processes take place at buried interfaces. Diffuse interfaces are important in adhesion, welding, crack healing, film integration, and the understanding of the macroscopic mechanical properties of composite structures. Indeed, interface development between two compatible polymers is a hot topic in polymer science at present—to take one example, in the case of films used in paper coating, latex paints and water-based adhesives, the properties of the particle–particle interface affects the performance of the resulting coating. Where spatial discrimination is not required, M-T DSC gives quantitative information on the formation of a diffuse interface, and allows the corresponding shift in glass transition temperature to be followed [98, 99]; a thermal method with the potential to determine the weight fraction and the thickness of the interface in multi-phase polymer materials has been described [100]. Using micro-thermal analysis it is now possible to investigate and quantify the mixing of material on a molecular level, which is crucial to the understanding of delamination processes.

A study by van Assche *et al* [101] has shown that micro-thermal analysis may be used to characterize interphases in thermoset-based composites, such as epoxies filled with glass beads or silica particles. It is argued that the results with these materials could provide a useful guide to how the properties of interphases in a wide range of composites, including fibre-reinforced polymers, blends and multilayer systems, may be measured. It is known that the development of such interphase regions often strongly affects the macroscopic properties of the composite material.

This work involved two types of measurement: the use of thermal imaging to detect gradients in heat transfer properties across an interphase, and L-TA at discrete points to observe spatial variations in local softening point or glass transition temperature (T_g). As illustrated in figure 26, for an anhydride-cured epoxy filled with (porous) silica particles, these particles are covered by resin, and the measurements were made at varying distances from the centre of a given particle. As this distance was *decreased* (and thus, as the volume of resin being analysed moves closer to the surface of the silica particle, see figure 26), two effects were seen: (figure 26(*b*)) values of softening point derived from L-TMA measurements decreased significantly; (figure 26(*d*)) the levels of the dc and ac imaging signals decreased also, indicating a gradient in thermal conductivity extending over the same distance as the change in softening point. The distance over which these quantities varied significantly from the bulk resin values was ca 70 μm. The decrease in softening point, and thus in T_g, corresponds to a reduced density of cross-linking. This (as confirmed by M-T DSC data) is caused by water diffusing into the curing matrix, and this affects the cross-linking polymerization process. The water originates from the

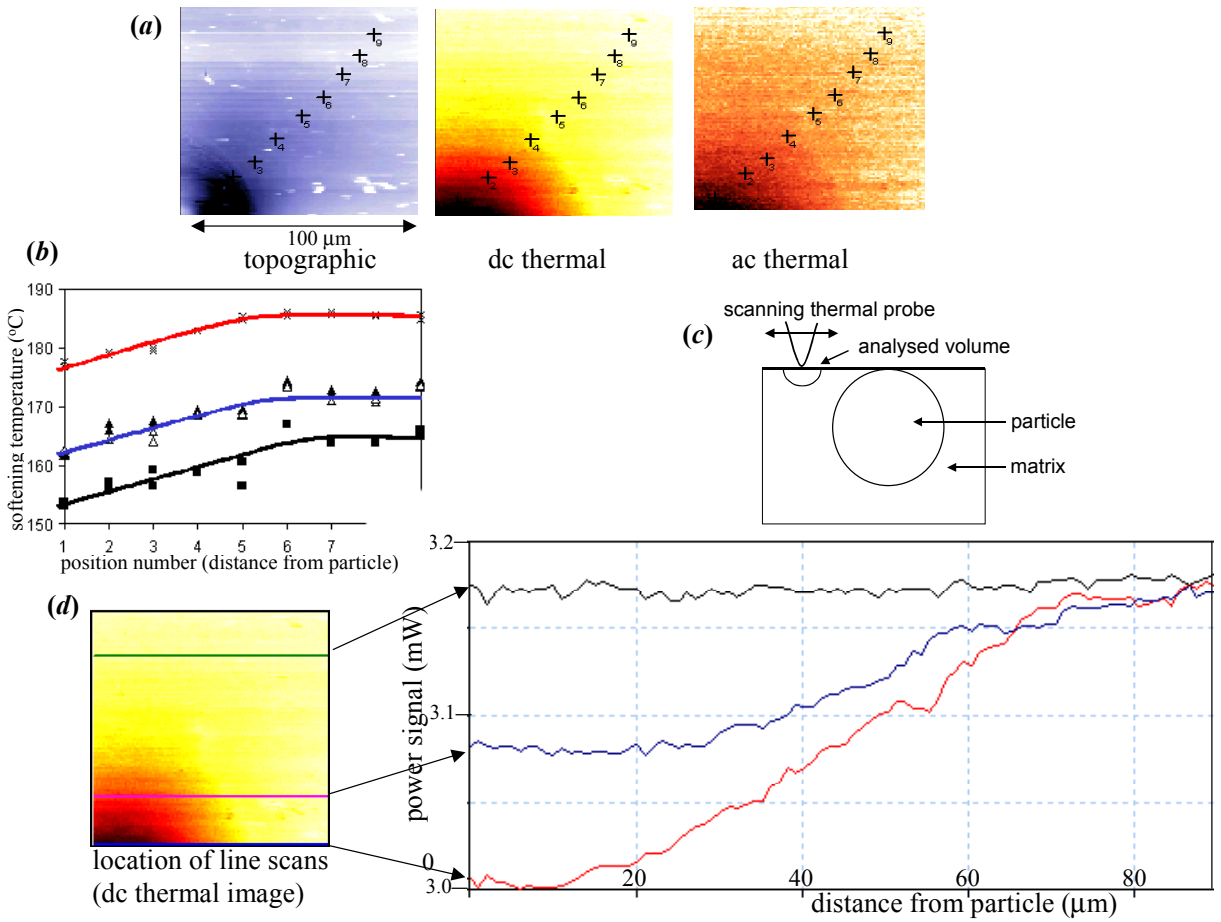

Figure 26. Interphases in a thermoset-based composite; an epoxy anhydride filled with silica particles. (*a*) The bottom left corner of the region shown in these SThM images is directly above the centre of a particle. Locations chosen for L-TMA scans are shown. (*b*) L-TMA results for local softening point of the epoxy anhydride filled with silica particles. The distance from the particle surface increases with increasing number. Data are for two lines of positions radiating from the same particle (as shown in (*a*): S, sensor signal; dS, derivative of sensor signal; ×, maximum of dS; ▲, dS at half peak height; △, S at onset of step; ■, dS at onset of peak). (*c*) Diagram showing a particle embedded in the matrix. (*d*) Line scans showing variation of dc thermal signal with distance from one of these silica particles. (After [101], copyright 2000 Dr G van Assche.)

silica particles which, being porous, contain ca 5% of adsorbed water when first introduced.

Häßler and zur Mühlen [67] have studied the degree of crystallinity and cross-linking behaviour of polymer material close to interfaces. Figure 27 shows thermal conductivity images of the cross section of an interface between acrylnitrile/polybutadiene/styrol polymer (ABS) and polyamide (PA). The polyamide is deposited as a sprayed coating at elevated temperatures onto sheets of ABS, and is required to adhere satisfactorily without delaminating. SThM images show a clear distinction between two types of sample, one rated 'satisfactory' and one 'faulty' as judged by the performance of the relevant coated sheets. L-TMA data were obtained from selected locations on the two samples, ranging from the ABS side across the interface to the polyamide side. For the 'satisfactory' sample, softening points rose from a value close to that of bulk ABS at ca 50 μm from the interface, to 490 K where a steep decrease in slope was seen as expected for the melting of polyamide. In between, this transition remains visible as the mixing with polyamide occurred, but at steadily decreasing softening temperatures. Curve 3 in particular shows the polyamide melt and, in addition, the intermediate softening point that confirms the presence of the separate phase of mixed material present in the interface. For the 'faulty' sample, as with the conductivity image, the transition as revealed by the curves is very abrupt; on the low conductivity side, and the softening point of ABS is seen at all points further than ca 10 μm from the interface. At that point the softening temperature is reduced by more than 30 K, suggesting a demixing of the components of the ABS. Between ABS and PA, a sharp boundary is visible in the thermal image, and the curves taken in the vicinity of the boundary show either ABS or PA behaviour. The lack of a shallow transition between the layers is most probably caused by a low processing temperature, with insufficient melting of the ABS surface. Given the significantly different values of thermal expansion coefficient for PA and ABS, it is to be expected that the components will delaminate.

Generally, the cross-linking density of a polymer is correlated with two parameters in particular: glass transition temperature (T_g) and thermal conductivity. Clearly, for a given sample, L-TA and SThM respectively will reveal variations in these quantities as a function of location. For example, microthermal analysis has been used to study how the properties of an aminic hardening epoxy on a DGEBA base epoxy resin varies

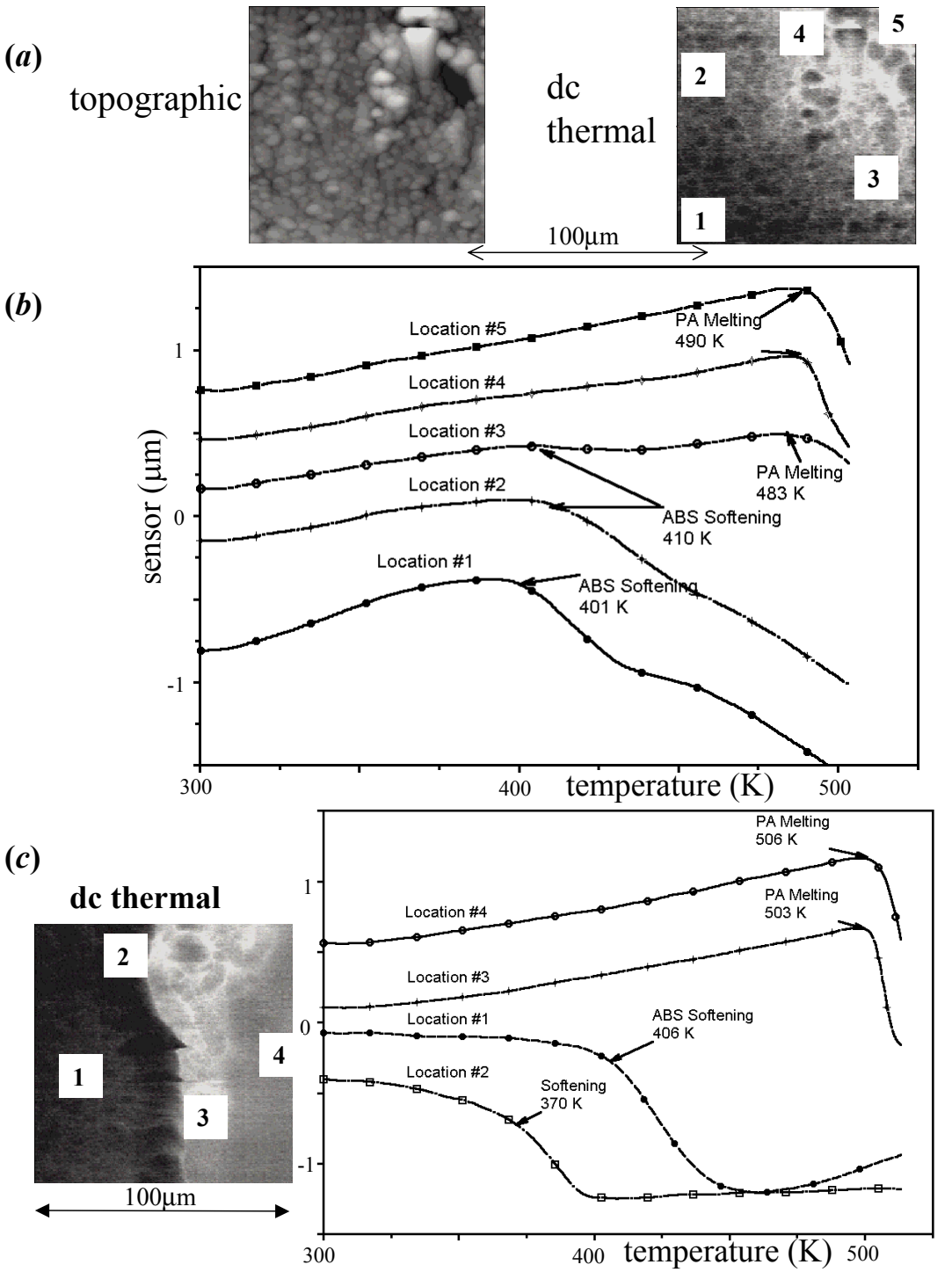

Figure 27. Interfaces between polymer and sprayed coatings. (*a*) Images of the cross section of an interface between acrylonitrile/polybutadiene/styrol polymer (ABS) and polyamide (PA). This sample was rated as 'satisfactory' as regards adhesion. The topographic image reveals only the quality of the surface after sample preparation, while the thermal image shows a slow and gradual change in conductivity, indicating that the interface is diffuse rather than sharp. (*b*) L-TMA data from the same interface, at locations shown by the numbers on the image. Curves obtained at locations 1 and 2 show how the softening points start at just above 400 K at ca 50 μm from the interface. Curves taken at locations 4 and 5 display the melting of PA at 490 K. Within the interface, curve 3 shows the polyamide melt and, in addition, an intermediate softening point, i.e. the softening of ABS as well as only a broad melting transition of PA can be observed. (*c*) For a 'faulty' sample, the thermal image shows a sharp and well-defined boundary between the two components. The L-TMA scans show that on the low conductivity side, the softening point of ABS is seen at all points further than ca 10 μm from the interface, at which point the softening temperature is reduced by more than 30 K. The individual curves show typical features of either ABS or PA transitions. (After [67], copyright 2000, with permission from Elsevier Science.)

with distance from an embedded glass fibre [67, 102]. The temperature of the softening transition of the resin is seen to rise at the fibre is approached, indicating an enhancement of the cross-linking density. Häßler and zur Mühlen also observe that the T_g of a two-component cold curing epoxy resin close to the interface with an oxidized aluminium sheet is 20 K higher than the bulk value; the oxidation treatment of the surface influences the cross-linking behaviour of the polymer.

In the section on localized thermo-rheometry we have seen how individual domains in a two-component phase-separated blend may be identified by means of pulsed force microscopy in combination with either a heating stage or localized heating. Using this technique, Reading [59] has shown that in the PS–PMMA system, an intermediate phase is revealed. Here it is necessary to take into account the possibility of a particular artefact; at phase boundaries, the probe can interact with more than one phase at a time. Fryer *et al* [103] have used L-CA to measure the glass transition temperature of thin films of photoresists and of their component materials (PS and PMMA) cast onto native silicon oxide substrates. They find that T_g is depressed by 10 °C (for PMMA) or more than 20 °C (for PS), when the film thickness is less than 70–80 nm. L-CA was also used to measure T_g for SAL605 photoresist films, in order to study the effect of the duration of post-apply bake. These data revealed the strong plasticizing effect of the solvent, and showed that the duration of post-apply bake should exceed 30 s at 90 °C to obtain consistent values of T_g in the film during processing.

5. Concluding remarks

As we have seen, polymer systems[5] have been involved in the majority of applications of micro-thermal analysis to date. The adaptability of the technique, and the variety of different versions, will encourage further expansion into other areas involving, for example, ceramics and biomedical materials. How rapidly this takes place depends on how soon the new developments become routinely available, in particular high-resolution micromachined probes, and instrumentation for localized photothermal spectroscopy, localized gas chromatography-mass spectrometry, scanning thermal expansion microscopy and localized thermo-rheometry.

As well as providing a tool for use in applied materials research, quantitative thermal microscopy and micro-thermal analysis could prove to be equally important in exploring wider questions of heat transfer at small lengths and timescales [1, 105] and in mesoscopic and low-dimensional systems.

Acknowledgments

The development of micro-thermal analysis would not have been possible without the continuing and inspiring collaboration of Mike Reading, who put forward the basic concept. Our particular thanks to him, to Guy van Assche, Laurent Bozec, Mike Conroy, Duncan Craig, Gero Fiege, Hartmut Fischer, Séverine Gomès, Rüdiger Häßler, Chris Hodges, Trevor Lever, Ekkehard zur Mühlen, Greg Meyers, Duncan Price, Rod Smallwood and Vladimir Tsukruk who all provided pre-publication material, and to Nancy Burnham, John Chalmers, Mike Claybourn, Neil Everall, Matt German, Dave Grandy, Philippe Grossel, Douglas Hourston, Bob Jones, Andrzej Kulik, Jezz Leckenby, Gordon Mills, Andrew Murray, Alastair Smith, Mo Song, Paul Turner and John Weaver. We thank the Engineering and Physical Sciences Research Council for funding, as well as T A Instruments Inc for additional financial support and Bruker UK for the loan of equipment.

[5] For a discussion of the future prospects of thermal analysis for the study of how heterogeneities on a (sub-)micrometre scale are often crucial to the behaviour and properties of polymer systems, see Mathot [104].

References

[1] Overney R M, Buenviaje C, Luginbuehl R and Dinelli F 2000 *J. Therm. Anal. Calorim.* **59** 205
[2] Williams C C and Wickramasinghe H K 1986 *Appl. Phys. Lett.* **49** 1587
[3] Williams C C and Wickramasinghe H K 1986 *Proc. 1986 Ultrasonics Symp.* ed B R McAvoy (New York: IEEE) p 393
[4] Nonnenmacher M and Wickramasinghe H K 1992 *Appl. Phys. Lett.* **61** 168
[5] Majumdar A, Carrejo J P and Lai J 1993 *Appl. Phys. Lett.* **62** 2501
[6] Williams C C and Wickramasinghe H K 1991 *J. Vac. Sci. Technol.* B **9** 537
[7] Luo K, Shi Z, Lai J and Majumdar A 1996 *Appl. Phys. Lett.* **68** 325
[8] Gimzewski J K, Gerber C, Meyer E and Schlittler R R 1994 *Chem. Phys. Lett.* **217** 589
[9] Nakabeppu O, Chandrachood M, Wu Y, Lai L and Majumdar A 1995 *Appl. Phys. Lett.* **66** 694
[10] K E Goodson and M Asheghi 1997 *Microscale Thermophys. Eng.* **1** 225
[11] Dinwiddie R B, Pylkki R J and West P E 1994 *Thermal Conductivity 22* ed T W Tong (Lancaster, PA: Technomics) p 668
[12] Majumdar A 1999 *Ann. Rev. Mater. Sci.* **29** 505
[13] Hammiche A, Pollock H M, Song M and Hourston D J 1996 *Meas. Sci. Technol.* **7** 142
[14] Balk L J, Maywald M and Pylkki R J *9th Conf. on Microscopy of Semiconducting Materials (Oxford) (Inst. Phys. Conf. Ser. 146)* pp 655–8
[15] Royall P G and Craig D Q M 2000 *Thermochim. Acta* to be published
[16] Zhou H, Midha A, Mills G, Thoms S, Murad S K and Weaver J M R 1998 *J. Vac. Sci. Technol.* B **16** 54
[17] Zhou H, Mills G, Chong B K, Midha A, Donaldson L and Weaver J M R 1999 *J. Vac. Sci. Technol.* A **17** 2233
[18] Mills G, Zhou H, Midha A, Donaldson L and Weaver J M R 1998 *Appl. Phys. Lett.* **72** 2900
[19] Dransfeld K and Xu J 1988 *J. Microsc.* **152** 35
[20] Xu J-B, Laeuger K, Moeller R, Dransfeld K and Wilson I H 1994 *J. Appl. Phys.* **76** 7209
[21] Gomès S, Trannoy N and Grossel P 1999 *Meas. Sci. Technol.* **10** 805
[22] Gorbunov V V, Fuchigami N, Hazel J L and Tsukruk V V 1999 *Langmuir* **15** 8340
[23] Luo K, Shi Z, Varesi J and Majumdar A 1997 *J. Vac. Sci. Technol.* B **15** 349
[24] Luo K, Herrick R W, Majumdar A and Petroff P 1997 *Appl. Phys. Lett.* **71** 1604
[25] Luo K, Lederman M and Majumdar A 1997 *Microscale Thermophys. Eng.* **1** 333
[26] Fischer H 2000 The m-TA (scanning thermal microscopy)—a tool for surface analysis and surface treatment *Presented at Highlights of Thermal Analysis: Applications Seminar (Würtzburg, Germany, 28/29 September 2000)*

[27] Hintzen H T, Fischer H, Breuls R and de With G 2001 in preparation
[28] Groenen R, Linden J L, Alcott G, Spee C I and Fischer H 2001 in preparation
[29] Hammiche, A, Reading M, Pollock H M, Song M and Hourston D J 1996 *Rev. Sci. Instrum.* **67** 4268
[30] Hammiche A, Hourston D J, Pollock H M, Reading M and Song M 1996 *J. Vac. Sci. Technol.* B **14** 1486
[31] Pollock H M, Hammiche A, Song M, Hourston D J and Reading M 1998 *J. Adhes.* **67** 217
[32] Pollock H M and Smith D A M 2001 *Handbook of Vibrational Spectroscopy* ed J M Chalmers and P R Griffiths (New York: Wiley) to be published
[33] Mills G, Conroy M, Hammiche A and Pollock H M 2001 submitted
[34] Almond D P and Patel P M 1996 *Photothermal Science and Techniques* (London: Chapman and Hall)
[35] Gmelin E, Fischer R and Stitzinger R 1998 *Thermochim. Acta* **310** 1
[36] Price D M, Reading M, Hammiche A and Pollock H M 1999 *Int. J. Pharmaceutics* **192** 85
[37] Oesterschulze E, Stopka M, Ackerman L, Sholtz W and Werner S 1996 *J. Vac. Sci. Technol.* B **14** 832
[38] Forster R and Gmelin E 1996 *Rev. Sci. Instrum.* **67** 4246
[39] Smallwood R, Metherall P, Hose D, Delves M, Pollock H M, Hammiche A, Hodges C S, Mathot V and Willcocks P 2001 *Thermochim. Acta* to be published
[40] Kreysig E 1993 *Advanced Engineering Mathematics* 7th edn (New York: Wiley)
[41] Depasse F, Gomès S, Trannoy N and Grossel P 1997 *J. Phys. D: Appl. Phys.* **30** 3279
[42] Gomès S, Depasse F and Grossel P 1998 *J. Phys. D: Appl. Phys.* **31** 2377
[43] Gomès S, Trannoy N, Grossel P, Depasse F, Bainier C and Charraut D 2001 *Int. J. Therm. Sci.* to be published
[44] Gomès S, Trannoy N, Depasse F and Grossel P 2000 *Int. J. Therm. Sci.* **39** 526
[45] Metherall P, Barber D C, Smallwood R H and Brown B H 1996 *Nature* **380** 509
[46] Varesi J and Majumdar A 1998 *Appl. Phys. Lett.* **72** 37
[47] Hammiche A, Price D M, Dupas E, Mills G, Kulik A, Reading M, Weaver J M R and Pollock H M 2000 *J. Microsc.* **199** 180
[48] Ruiz F, Sun W D, Pollak F H and Venkatraman C 1998 *Appl. Phys. Lett.* **73** 1802
[49] Gorbunov V V, Fuchigami N and Tsukruk V V 2000 *Probe Microsc.* **2** 65
[50] Callard S, Tallarida G, Borghesi A and Zanotti L 1999 *J. Non-Cryst. Solids* **245** 203
[51] Moon I K, Jeong Y H and Kwun S I 1996 *Rev. Sci. Instrum.* **67** 29
[52] Cahill D G 1990 *Rev. Sci. Instrum.* **61** 802
[53] Moon I, Androsch R, Chen W and Wunderlich B 2000 *J. Therm. Anal. Calorim.* **59** 187
[54] Fiege G B M, Altes A, Heiderhoff R and Balk L J 1999 *J. Phys. D: Appl. Phys.* **32** L13
[55] Carslaw H S and Jaeger J C 1947 *Conduction of Heat in Solids* (Oxford: Clarendon) p 193
[56] Haines P J (ed) 1995 *Thermal Methods of Analysis: Principles, Applications and Problems* (London: Blackie) pp 123–60
[57] Price D M, Reading M, Hammiche A and Pollock H M 2000 *J. Therm. Anal. Calorim.* **60** 723
[58] Reading M, Price D M, Grandy D B, Smith R M, Bozec L, Conroy M, Hammiche A and Pollock H M 2001 *Macromolecular Symposia 2001* **167**
[59] Reading M 2001 *Thermochim. Acta* submitted for publication
[60] Weilandt E, Hild S and Marti O 1997 *Meas. Sci. Technol.* **8** 1333
[61] Price D M, Reading M, Hammiche A, Pollock H M and Branch M G 1999 *Thermochim. Acta* **332** 143
[62] Hammiche A, Bozec L, Conroy M, Pollock H M, Mills G, Weaver J M R, Price D M, Reading M, Hourston D J and Song M 2000 *J. Vac. Sci. Technol.* B **18** 1322
[63] Tian M-W, Loos J and Fischer H 2001 in preparation
[64] Gorbunov V V, Fuchigami N and Tsukruk V V 2000 *High Perform. Polym.* **12** 603
[65] Reading M 1993 *Trends Polym. Sci.* **1** 248
[66] Jones K J, Kinshott I, Reading, M, Lacey A A, Nikolopoulos C and Pollock H M 1997 *Thermochim. Acta* **305** 187
[67] Häßler R and zur Mühlen E 2000 *Thermochim. Acta* **361** 113
[68] Pollock H M 1992 Surface Forces and Adhesion *Fundamentals of Friction* ed I L Singer and H M Pollock (New York: Kluwer) pp 77–94
[69] Grandy D B, Hourston D J, Price D M, Reading M, Goulart Silva G, Song M and Sykes P A 2000 *Macromolecules* **33** 9348
[70] Binnig G, Despont M, Drechsler U, Häberle W, Lutwyche M, Vettiger P, Mamin H J, Chui B W and Kenny T W 1999 *Appl. Phys. Lett.* **74** 1329
[71] Price D M, Reading M, Smith R M, Hammiche A and Pollock H M 2001 *J. Thermal Anal. Calorim.* **64** 309
[72] Price D M 2000 *Presented at 2nd Int. Micro-TA Symp. (Western Kentucky University, USA, 8/9 May 2000)*
[73] Rosencwaig A 1980 *Photoacoustics and Photoacoustic Spectroscopy* (New York: Wiley)
[74] Bialkowski S E 1996 *Photothermal Spectroscopy Methods for Chemical Analysis* (New York: Wiley)
[75] Williams C C and Wickramasinghe H K 1998 *Soc. Photogr. Instrum. Eng.* **897** 129
[76] Grafstrom S, Kowalski J, Neumann R, Probst O and Wortge M 1991 *J. Vac. Sci. Technol.* B **9** 568
[77] Trannoy N, Grossel P and Troyon M 1998 *Probe Microsc.* **1** 201
[78] Oesterschulze E, Stopka M and Kassing R 1994 *Microelectron. Eng.* **24** 107
[79] Anderson M S 2000 *J. Appl. Spectrosc.* **54** 349
[80] Stranick S J, Cavanagh R R, Chase D B, Jordan C E, Michaels C A and Richter L J 1999 *Preliminary Proc. STM '99 (Seoul, Korea, 19–23 July 1999)* ed Y Kuk *et al* (Seoul: Seoul National University) p 226
[81] Bozec L, Hammiche A, Pollock H M, Conroy M, Chalmers J M, Everall N J and Turin L 2001 to be published
[82] Hammiche A, Pollock H M, Reading M, Claybourn M, Turner P H and Jewkes K 1999 *Appl. Spectrosc.* **53** 810
[83] Price D M, Reading M and Lever T J 1999 *J. Therm. Anal. Calorim.* **56** 673
[84] Song M, Hourston D J, Pollock H M, Schäfer F U and Hammiche A 1997 *Thermochim. Acta* **304** 335
[85] Siggia E D 1979 *Phys. Rev.* A **20** 595
[86] Murray A, Lever T, Reading M and Price D 1998 *Mater. World* **6** 615
[87] Royall P G, Craig D Q M, Price D M, Reading M and Lever T J 1999 *Int. J. Pharmaceutics* **190** 97
[88] Royall P G, Hill V L, Craig D Q M, Price D M and Reading M 2000 *Pharm. Res.* at press
[89] zur Mühlen E 1999 *Developments in Polymer Analysis and Characterisation (papers from seminar 10 May 1999)* (Rapra Technology Ltd)
[90] Price D M, Reading M, Caswell A, Hammiche A and Pollock H M 1998 *Microscopy and Analysis* **65** (May) 17
[91] Royall P G, Kett V L, Andrews C S and Craig D Q M 2001 *J. Phys. Chem.* to be published
[92] Sanders G H W, Roberts C J, Danesh A, Murray A J, Price D M, Davies M C, Tendler S J B, Williams P M and Wilkins M J 2000 *J. Microsc.* **198** 77
[93] Grandy D 2001 *Thermochim. Acta* to be published
[94] Price D M, Reading M, Lever T J, Hammiche A and Pollock H M 2001 *Thermochim. Acta* **367–8** 195
[95] Hodges C S 1999 *PhD Dissertation* Lancaster University
[96] Buck A, Jones B K and Pollock H M 1997 *Microelectron. Reliab.* **37** 1495

[97] Meyers G F, Dineen M T, Shaffer II E O, Stokich T Jr and Im J-H 2000 *Polym. Prepr. (Am. Chem. Soc., Div. Polym. Chem.)* **41** 1419
[98] Song M, Hammiche A, Pollock H M, Hourston D J and Reading M 1995 *Polymer* **36** 3313
[99] Hourston D J, Song M, Hammiche A, Pollock H M and Reading M 1997 *Polymer* **38** 1
[100] Song M, Pollock H M, Hammiche A, Hourston D J and Reading M 1997 *Polymer* **38** 503
[101] Van Assche G, Volckaerts B and Van Mele B 2000 *Presented at 2nd Int. Micro-TA Symp. (Western Kentucky University, USA, 8/9 May 2000)*
[102] Haessler R 2000 *Presented at Highlights of Thermal Analysis: Applications Seminar (Würtzburg, Germany, 28/29 September 2000)*
[103] Fryer D S, dePablo J J and Nealey P F 1998 *Proc. SPIE* **3333** 1031
[104] Mathot V B F 2000 *Thermochim. Acta* **355** 1
[105] Shi L, Plyasunov S, Bachtold A, McEven P L and Majumdar A 2000 *Appl. Phys. Lett.* **77** 4295